INTEGRATIVE LATERALITY MAPPING WITH MEG AND FMRI FOR PRESURGICAL EVALUATION IN EPILEPSY

by

Sean R. McWhinney

Submitted in partial fulfillment of the requirements

for the degree of Master of Science

at

Dalhousie University

Halifax, Nova Scotia

September 2013

Table of Contents

List of Tables

List of Figures

Abstract

Temporal lobe epilepsy reflects the single most common cause of refractory epilepsy, and seizures can be controlled in many cases by anterior temporal lobe resection. However, proximity of epileptogenic tissue to regions involved in language and memory processing means the potential impact of surgery on these abilities must be addressed. Currently-used laterality assessments establish hemispheric dominance, but are unable to determine dominance within a particular region. This is problematic as people with epilepsy more commonly demonstrate atypical distribution of language functioning in the brain. Finer-grained assessments use functional magnetic resonance imaging (fMRI), but they often suffer signal distortion in temporal lobe regions due the presence of airways. Magnetoencephalography (MEG) shows a complimentary sensitivity in such problematic regions, but has not been used for laterality assessment. We present a method that combines fMRI with MEG for optimized sensitivity across the brain. In addition, a laterality assessment is described that depicts laterality at a high spatial resolution. Combined, these advances allow for more comprehensive definition of laterality across the brain. MEG activation maps were generated using a signal space separation beamformer, showing activation in anterior temporal lobe regions and lateral occipital cortex. fMRI showed activation in a network of medial temporal lobe regions and in frontal poles, and in the hippocampus, an area of clinical concern during surgical planning. The present study introduces a method for integrating MEG and fMRI activation to create high-resolution laterality maps in regions of concern for epilepsy.

List of Abbreviations Used

CLV	Complex laterality vector
EEG	Electroencephalography
fMRI	Functional magnetic resonance imaging
HRF	Hemodynamic response function
LI	Laterality index
MEG	Magnetoencephalography
MRI	Magnetic resonance imaging
PET	Positron emission tomography
SMA	Supplementary motor area

Acknowledgements

I would like to express my gratitude toward my supervisors Dr. Ryan C.N. D'Arcy and Dr. Aaron Newman for their support of this research, dedication to my success, and guidance in bringing this research to its full potential. In addition, I would like to thank the rest of my thesis committee, Dr. Antonina Omisade, and Dr. Olav Krigolson, for their insight and expertise. Additional thanks go to Graham Little for assistance with the small but critical technical obstacles, and to Dr. Timothy Bardouille and Dr. Antoine Tremblay for lending their analytical knowledge and skill.

1 Introduction

1.1 Presurgical Evaluations in Epilepsy

The various forms of epilepsy are commonly characterized by recurrent and unprovoked seizures, resulting from abnormal or excessive neural firing in the brain (Fisher et al., 2005). It has recently been estimated that there are 50 million people with epilepsy worldwide ("Epilepsy," 2012). Additionally, epilepsy becomes more common with age (Brodie, Elder, & Kwan, 2009), making it a primary concern for Canada's aging population ("CANSIM Table 051-0001," 2012). Anterior temporal lobe resection has become the standard of care for refractory temporal lobe epilepsy. One study reports seizure-free surgery outcomes in 60% of anterior temporal lobe resections, while only 8% of people experienced no seizures using medications (Wiebe, Blume, Girvin, & Eliasziw, 2001). Anterior temporal lobe resection methods vary regarding the amount of tissue removed, depending on the location of epileptogenic tissue, seizure severity and frequency, and proximity of epileptogenic tissue to regions serving cognitive functions such as language and memory. Techniques range from selective amigdalohippocampectomy to more severe resection of lateral temporal cortex along with medial structures (Al-Otaibi, Baeesa, Parrent, Girvin, & Steven, 2012). Evaluation is made on an individual basis with careful consideration for surgical outcomes.

The likelihood of outcomes, both positive (fewer or no seizures) and negative (reduction in processing abilities), is predicted through presurgical evaluation. The

ability to appropriately weigh these outcomes is of critical concern, and may drastically impact an individual's outcome and therefore quality of life following surgery. To determine whether the hemisphere of surgical focus coincides with the laterality of critical functions, language and memory laterality are commonly assessed. A number of commonly used laterality assessments exist for different types of cognitive functions. For example, a dichotic listening task is commonly used to lateralize speech perception dominance to a hemisphere (Ingram, 2007). In this type of assessment, participants are presented with two speech stimuli simultaneously, one to each ear. A performance advantage to one ear indicates preferential processing in the opposing hemisphere. This task is intended to provide a measure of laterality, indicating either left or right hemispheric dominance in speech perception. This type of information can be useful and is often used in clinical evaluations.

Similarly, the gold standard in language and memory laterality assessments remains the intracarotid sodium amobarbitol procedure, or Wada test (Wada, 1949). This test introduces a barbiturate (commonly sodium amobarbitol) into one hemisphere, inhibiting central nervous system functioning at the site of administration. The Wada test typically involves administering the barbiturate via femoral catheter into the carotid artery. Initially, this test was developed to reduce the cognitive side effects associated with bilateral electroconvulsive therapy, with findings reported on motor, sensory and language functions (Wada, 1949). The test has since been extended for use as a language laterality assessment. Following barbiturate administration, neuropsychological testing can be carried out in order to

determine hemispheric dominance for language and memory processing. In addition to invasiveness, this test suffers similar limitations regarding spatial distribution to the dichotic listening task.

Laterality assessments often report a laterality index (LI) as the result. The LI serves as an indication of hemispheric dominance (left, right or bilateral) by comparing the contributions of each hemisphere (Desmond et al., 1995). During Wada and neuropsychological testing, the contributions of each hemisphere are scored. The two are contrasted and then divided by their combined score, resulting in a single number that indicates left hemisphere (+1), right hemisphere (-1) or bilateral (0) dominance. Traditional laterality assessments are most useful when there is a clear separation between hemispheric dominance and the planned region of resection. However, results can be more difficult to interpret when this is not the case.

The primary limitation of the LI is its inability to address the distribution of active regions within each hemisphere, instead reflecting the larger-scale contributions of each. This is often a concern as temporal lobe epilepsy is the most common cause of refractory epilepsy (Wiebe, 2000), and numerous anatomically and functionally distinct regions of the temporal lobe serve roles in language and memory processing (J. R. Binder et al., 1997; Maess, Herrmann, Hahne, Nakamura, & Friederici, 2006; Newman, Pancheva, Ozawa, Neville, & Ullman, 2001). When critical functions are lateralized to the hemisphere of surgical focus, a finer-grained evaluation is necessary to predict surgical outcomes.

The coarse nature of the laterality index may be a result of our historically poor ability to localize epileptogenic regions. Localization is typically done using electroencephalography (EEG) to measure interictal spiking and seizure activity. The EEG signal is heavily distorted by brain, fat and scalp tissue, contributing to poor spatial resolution (Nunez & Srinivasan, 1981). Use of depth electrodes or cortical electrode meshes placed under the skull can achieve ideal accuracy, but are highly invasive. Thus, non-invasive localization of epileptogenic regions has most commonly been performed on an inherently coarse scale, and fine-grained localization of language and memory functions would provide little benefit when considered against these measures.

1.2 Neuroimaging in Presurgical Evaluation

Numerous neuroimaging technologies have greatly augmented our capacity to localize functional and epileptogenic regions with a high degree of accuracy. Most commonly, functional mapping has been carried out using functional magnetic resonance imaging (fMRI). Functional MRI activation is derived from blood oxygen level dependent (BOLD) signals, which reflect a change in the proportion of oxygenated to deoxygenated hemoglobin. Due to an excess of blood supply, changes in blood oxygenation occur on a scale larger than regions of neural activity, but can still be localized on the order of millimeters (Fox & Raichle, 1986). The most prominent use for fMRI has been for functional mapping of a number of neural systems spanning the cortex (Appel et al., 2013; Williams et al., 2012). Most commonly, this has included motor and somatosensory regions (Majos, Tybor, Stefanczyk, & Goraj, 2005; Roux et al., 2000). fMRI has also been used to establish

the functional status of the hippocampus in each hemisphere, as this structure is involved in a number of memory-related processes (Bonelli et al., 2010; Sidhu et al., 2013; Squire, 1992; Stretton et al., 2012). Disentangling hippocampal activity from epileptogenic regions is a primary concern when evaluating individuals with temporal lobe epilepsy for surgery. Additionally, its proximity to the commonly resected anterior temporal lobe marks the hippocampus for careful consideration (Bonelli et al., 2010, 2011; Sidhu et al., 2013; Stretton et al., 2012).

Many centres around the world also have begun using magnetoencephalography (MEG) for functional mapping. MEG measures magnetic fields generated by the brain to estimate the location and magnitude of neural activity. There is a growing body of research to demonstrate the ability of MEG to localize functional regions at a resolution comparable to that of fMRI. Most notably, this includes mapping of motor and somatosensory cortices (Oishi et al., 2002), as well as language regions (D'Arcy et al., 2013; Grummich, Nimsky, & Pauli, 2006; Leonard et al., 2013; Pang, Wang, Malone, Kadis, & Donner, 2011).

Regions of the brain associated with seizure onset have commonly been delineated using both MRI and MEG. One study used high-field MRI to identify hippocampal sclerosis in people with epilepsy with temporal lobe epilepsy (TLE) (Henry, Strupp, & Sikora, 2011). Such instances of mesial hippocampal atrophy have been associated with seizure onset (Finegersh et al., 2012). While there is not always a one-to-one correspondence between atrophied regions and the location of seizure onset, the location of these malformations is often instructive, and this information is often used in conjunction with other assessments to develop a more

comprehensive presurgical evaluation. These findings have been aided by developments such as increased field strength, which have resulted in greater resolution and image contrast. However, people with epilepsy with electrophysiological evidence for temporal lobe epilepsy show no abnormalities with MRI in 30% of cases (Cascino et al., 1991).

In these and other cases, applying MEG source modeling solutions to measurements of magnetic fields generated during spiking activity allows for localization of epileptogenic regions. A wide variety of such solutions exist, including equivalent current dipole (ECD) models, minimum norm estimation, and a multitude of dynamic statistical parametric mapping procedures. While each has benefits and disadvantages, ECD models have commonly used to localize interictal spiking (Jeong, Chung, & Kim, 2012). These models assume single sources of neural activity rather than networks of activation, making them a natural fit for spike detection. More recently, algorithms have been developed to detect and map degrees of brain-wave kurtosis across the brain, as exhibited during spiking (Vrba, Taulu, & Nenonen, 2010). While promising, kurtosis mapping is still experimental and is not used clinically.

Availability of non-invasive, high-resolution neuroimaging modalities calls for more specific laterality assessments, which cannot be accomplished using traditional means. The proximity of temporal lobe regions involved in language and memory processing to the commonly resected anterior temporal lobe warrants careful consideration, particularly when functional laterality and seizure onset share a hemisphere. Importantly, each of the technologies discussed above has inherent

limitations that hinder their abilities to assess laterality in these regions. However, these abilities are complementary, and may compensate for one another.

1.3 Applications and Limitations of Functional MRI

The change in hemodynamics following a neural event has been precisely modeled and is active for twelve to sixteen seconds following neural activity (Chen & Li, 2012). This time course varies only minimally depending on region and has been well modeled across the brain; Changes in the amplitude of the BOLD response are mostly seen when comparing gray and white matter, rather than different regions of the cortex (Rostrup et al., 2000). For these reasons, fMRI can be considered a temporally precise, but also coarse measure or neural activity.

Functional magnetic resonance imaging (fMRI) has become widely used in functional mapping and laterality assessments globally (Bahn et al., 1997; J. Binder et al., 1996; Desmond et al., 1995; Hertz-Pannier et al., 1997; Woermann et al., 2003). While its major appeal is high spatial resolution and specificity, fMRI has limitations inherent in its design. For example, the BOLD signal can be distorted by inhomogeneities in the magnetic field. This is most notable in regions where the densities of neighboring tissues differ, causing magnetic susceptibility artifact. This artifact is particularly prominent in medial inferior frontal lobes (near sinuses and the oral cavity), as well as anterior temporal lobes (above the ear canals). However, medial temporal regions including the hippocampus are not as strongly affected (Eldridge, Engel, Zeineh, Bookheimer, & Knowlton, 2005).

Functional MRI is also sensitive to artifacts induced by participant motion, and to other sources of physiological noise including respiration and cardiac effects

(Zeffiro, 1996). Additionally, people with epilepsy with pace makers, metallic implants or pins are unable to enter the scanning environment for their own safety. While fMRI is non-invasive and spatially precise, it is not appropriate for all populations. Signal distortion in temporal lobe regions often considered for resection is also a concern, as critical activity in these regions may be lost (Devlin et al., 2000). This is likely to result in an unnecessary reduction in language or memory abilities following surgery (Al-Otaibi et al., 2012). Where the value of fMRI can be limited for certain applications, MEG shows promise.

1.4 MEG and Electrophysiology

MEG has been used increasingly for presurgical evaluation of epilepsy people with epilepsy (Bowyer et al., 2005; Breier et al., 2005; D'Arcy et al., 2012; Lee et al., 2006; Papanicolaou et al., 1999). MEG uses arrays of superconducting quantum interference devices (SQUIDs) to measure local changes in magnetic fields. There are two types of commonly-used SQUIDS, magnetometers and axial gradiometers. While magnetometers are designed to record the strength of a magnetic field at their location, gradiometers instead measure the change in a field across a gradient. In the MEG scanner used in the present study, sensors are arranged in triplets (two gradiometers, one magnetometer) across a helmet-shaped configuration, as shown in Figure 1. The MEG system is located in a magnetically shielded room which employs passive deterring of external magnetic fields, as well as active shielding via noise cancellation.

Post-synaptic potentials created by neural firing generate a magnetic field, which forms a counterclockwise pattern, perpendicular to the direction of the

neural activity. While magnetic fields are also generated by axonal conduction, their magnitude is greatly overshadowed by that of the fields generated by postsynaptic potentials due to the number of synaptic connections in the brain. If the circular field encompasses one or more SQUID sensors, it in turn induces a current on the sensor. This measurement can then be used to localize the source of activity.

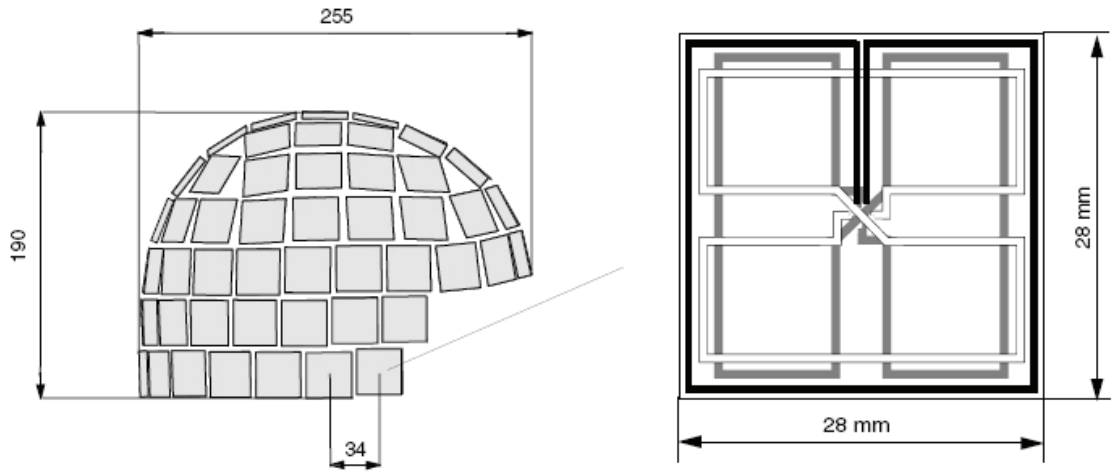

Figure 1 The sensor array of an Elekta Neuromag MEG system, showing the helmet configuration (left) and the triplet arrangement of SQUID sensors (right).

1.5 Field Distribution and Source Localization

The largest difficulty in localization of neural activity using MEG has historically come from the inverse problem, which is mathematically ill-posed: An unlimited number of source configurations have the potential to generate any given magnetic field distribution. Figure 2 depicts this dilemma.

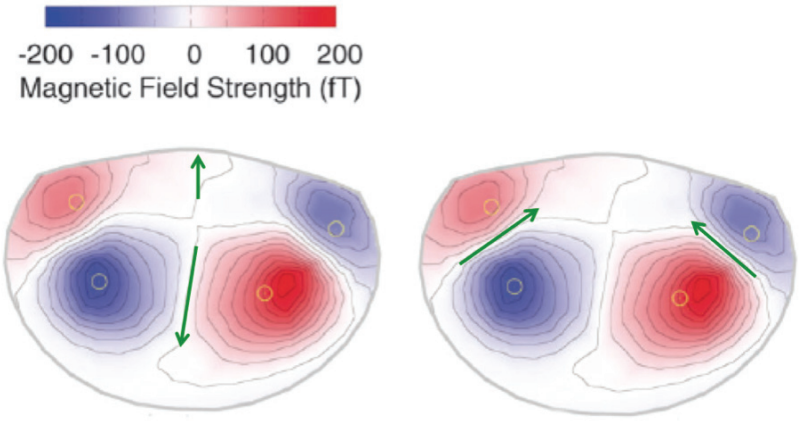

Figure 2 A sample magnetic field distribution, adapted from Ross et al. (2009). Two possible source configurations are shown (left and right), demonstrating the inverse problem. Potential sources are represented as dipoles using green arrows.

While the inverse problem was initially thought to be insurmountable, various methods now exist to estimate which source configuration accounts for the highest proportion of the measured variance, allowing for inference as to the probability of various configurations. These methods are capable of generating high-resolution spatiotemporal activation maps. Minimum norm estimation is a method commonly used for distributed source localization, which estimates the probability that an observed magnetic field could be generated by a number of singular points of activation across the cortical surface. Because source depth is not depicted, maps can be considered two-dimensional (Hamalainen & Ilmoniemi, 1994). Alternatively, beamformer algorithms generate a series of sensor weighting profiles that act as spatial filters, attenuating signals except those for a voxel of interest and estimating signal magnitude (Sekihara, Nagarajan, Poeppel, & Marantz, 2004). This calculation is performed iteratively across the brain and produces volumetric output comparable to that commonly generated using fMRI. The present study uses a signal

space separation beamformer, which further attenuates signals originating outside the MEG helmet (Vrba et al., 2010).

MEG has been used for source localization in a vast number of research areas. These include interictal spike mapping for epilepsy (Jeong et al., 2012), distributed localization of complex networks (Cornelissen et al., 2009), and somatosensory system mapping in schizophrenia (Huang et al., 2010). The growing body of MEG research indicates that its use for functional mapping is being recognized in centres around the world. However, it should be noted that magnetic field strength reduces with distance from neural activity. For this reason, MEG is best suited to detect sources of neural activity in cortical regions. As has been discussed, the hippocampus plays a crucial role in language and memory functioning, and its functional status is commonly assessed during presurgical evaluation (Bonelli et al., 2011; Stretton et al., 2012). While MEG is not hindered by activation near sinuses and other regions that are problematic for fMRI (lateral and anterior temporal regions), a powerful experimental design is necessary to isolate hippocampal signals. For functions spanning a range of temporal regions, a laterality assessment capable of incorporating both modalities is necessary.

1.6 Multimodal Integration

MEG and fMRI are both capable of high-precision estimation of neural activity, but possess spatially complementary sensitivity profiles. The limitations of the two imaging methods make using either one alone potentially suboptimal for laterality assessments that involve anterior and medial temporal regions. In

consideration of this, there have been a number of developments toward integrating MEG and fMRI data to produce a single, highly sensitive functional mapping technique.

A clear challenge to the integration of fMRI and MEG is that they measure different things. Beyond differences in regional sensitivity, fMRI measures blood oxygenation secondary to neural activity, while MEG measures current flow among large groups of synchronously-active neurons. One study demonstrated that local field potentials, which include neural input and internal functioning, correlate more highly with the BOLD signal than post-synaptic output (Logothetis, Pauls, Augath, Trinath, & Oeltermann, 2001). Conversely, MEG is more sensitive to postsynaptic activity, in particular that which occurs closest to the cortical surface (Nunez & Srinivasan, 1981). However, MEG and fMRI data have demonstrated close co-localization (Pang et al., 2011). One study has found that in 172 people with epilepsy, localization of Broca's area and Wernicke's area using MEG coincided their locations as identified using fMRI in 96% of cases (Grummich et al., 2006). However, these are regions not known to be strongly affected by magnetic susceptibility artifact using fMRI, or signal loss due to depth using MEG. There are additional considerations regarding signal magnitude, however. It is known that the relationship between neural activity and BOLD is non-linear, and is modulated by the rate of neural firing and the period of time over which stimuli are presented (Rees et al., 1997). Because the generation of magnetic fields is the result of electric discharge, neural firing both in terms of rate and the number of active neurons show a linear relationship with the magnitude of the magnetic field being generated. For

these reasons, changes in stimulus timing or duration are likely to induce signal changes of varying magnitude depending on modality, confounding contrasts that rely on such factors. Therefore, consistency of these conditions must be maintained as not to induce differences in contrast magnitude that are specific only to one modality.

A common approach to combining fMRI and MEG is to use fMRI activation locations to constrain the source localization of MEG data. This approach is taken because fMRI localization is generally taken as highly reliable (with the exceptions noted above), while MEG source localization is more dependent on various assumptions and thus has more variable outcomes. For example, Henson et al. (2010) have proposed a method of combining fMRI and MEG activation that weights the two maps asymmetrically. Using this method, each cluster of fMRI activation is treated as a unique prior during fusion with MEG activation maps. This allows the fMRI data to influence MEG activity, regardless of the time at which MEG activity occurs, effectively collapsing the time components of MEG data. Henson et al. (2010) admit that neither data set should constrain the other in an optimal model of integration. However, they state it is more practical to constrain regions of MEG activity by active fMRI clusters in this manner until this relationship between fMRI and MEG signals is better understood.

Similarly, Freeman at al. (2009) proposed a model in which MEG time series data are calculated across the brain, and signal power in the beta and gamma bands are correlated with fMRI signal intensity at that location. This method is sensitive to regions that are active in both modalities, but neglects activity measured only in one.

While these approaches demonstrate solutions to timing-related concerns, regional sensitivity differences remain a major concern. Liu et al. (2006) have demonstrated that fMRI-invisible sources of activity are the most problematic factors in fMRI-constrained integration of fMRI and MEG/EEG data. Loss of power to fMRI-invisible sources can be countered by using modified integration algorithms, but this instead results in insensitivity to fMRI-extra regions (Liu et al., 2006). Together, these studies demonstrate that there is no reliable method to constrain MEG activity to fMRI-active regions. Instead, the two should be given appropriate degrees of influence over an integrated activation map.

1.7 Approach to Integration in the Current Study

Applying the constraints outlined above dismisses all spatial capabilities of MEG, rather than weighing them appropriately. When combined with known fMRI-invisible sources across temporal regions involved in language and memory, this is detrimental to surgical outcomes. Now that error resulting from the inverse problem can be estimated for MEG, spatial information can be appropriately incorporated. A new presurgical laterality assessment has been developed that combines, rather than constrains, MEG and fMRI data. This method integrates the two using a data-driven measure of confidence at each region for optimal sensitivity in problematic areas.

Data from a language-based visual object working memory task was used to develop an approach to the integration of MEG and fMRI data across the brain, including areas that pose problems to each, such as the hippocampus and anterior temporal lobes. MEG data were localized using a signal space separation

beamformer (Vrba et al., 2010). Using this type of task engages numerous neural systems, including multiple visual perception streams, lexical access for object naming, and working memory encoding. The task leverages both spatial and verbal aspects of object naming, involving areas known to be problematic for both imaging modalities. Conversely, a task that relies purely on auditory or read language input is likely to engage fewer regions, and may be less suitable for examining regional differences in multimodal integration. MEG and fMRI data were spatially normalized, and contrast-to-noise ratios (CNR) were calculated across the brain using each data set. The CNR was then used to weight the integration of MEG and fMRI data at each voxel, providing more weight to the modality most sensitive to activity in that region. The laterality of active regions was then examined using both traditional and recently established laterality measures (D'Arcy et al., 2013).

Using a similar task, Bar and colleagues (2001) showed fMRI activation in inferior temporal regions of the left hemisphere including the fusiform gyrus and parahippocampal gyrus, with additional activation in the inferior frontal gyrus. Right-hemisphere activation was also shown in the right fusiform gyrus. As well, a bilateral network of lateral occipital regions has shown involvement in identification of intact objects (Grill-Spector, Kourtzi, & Kanwisher, 2001). Finally, the hippocampus receives inputs from the perirhinal and entorhinal cortices, both of which show left-lateralized activation during recognition of complex objects (Bellgowan, Buffalo, Bodurka, & Martin, 2009). In light of these findings, a similar network of activation was expected in the present study. Both healthy control participants and individuals with epilepsy completed the task. The purpose of the

study was to advance laterality assessment by examining laterality individually for active regions, and by integrating multimodal data to create a maximally sensitive depiction of laterality.

1.8 Objectives

- To further develop our laterality mapping procedure in healthy controls and in people with epilepsy with epilepsy, by extending the procedure to depict laterality in deep structures including the hippocampus.
- To develop a novel method for creating combined MEG-fMRI laterality maps.
- To evaluate differences in regional sensitivity across modalities, and to investigate the effects of combining MEG and fMRI in a number of regions.

1.9 Hypotheses

- Activity will be localized to the inferior prefrontal cortex, fusiform gyrus, parahippocampal gyrus, hippocampus, and lateral occipital cortex. Activation will predominantly show left-hemisphere lateralization.
- Sensitivity is expected to be higher in MEG than in fMRI maps in the anterior temporal lobes. Conversely, sensitivity is expected to be higher in fMRI than in MEG maps for the hippocampus.
- Integrated activation maps will show activity in regions found active using MEG but not fMRI, and in regions found active using fMRI but not MEG.

2 Methodology

2.1 Participants

Participants included 10 neurologically intact adults (4 male) with a mean age of 28.4 years (range = 20 – 48; SD = 9.3), and 13 people with epilepsy with epilepsy (5 male), with a mean age of 30.8 years (range = 13 - 49; SD = 10.4). There was no significant difference in ages between the two groups ($t(21) = .53$). All participants were right handed, as assessed using the Edinburgh Handedness Inventory (Oldfield, 1971), except for one person with epilepsy. People with epilepsy were referred to the study from the Epilepsy Monitoring Unit at the Halifax Infirmary by their neurologist. Clinical and demographic information for people with epilepsy is provided in Table 1; some information was unavailable for some participants. All participants were fluent in English, had normal or corrected to normal vision, and provided informed consent to participate. The IWK Health Centre and National Research Council Canada research ethics boards approved this research.

Table 1 Clinical and demographic information for people with epilepsy

Sex	Age	Onset	Diagnosis	EEG	MRI	Medication
F	30	5	Symptomatic cortical dysplasia Focal onset, secondary generalized	Scalp: F3-FZ spikes; FZ onset seizures; Stereotactic depth EEG: Seizure onset within the cortical dysplasia	Left frontal cortical dysplasia	Levetiracetam, Lamotrigine
F	39	25	Symptomatic malformation of cortical development	Scalp EEG: Right frontal spikes, seizures. Subdural EEG: seizure onset right orbital frontal	Right orbital frontal malformation of cortical development	Levetiracetam, Lamotrigine
F	49	39	Idiopathic epilepsy	Scalp EEG: Left temporal spikes, seizures	Normal	Divalproex, Lacosamide
F	13	--	--	--	--	--
M	20	10	Idiopathic epilepsy	Scalp EEG: Generalized polyspike and wave	Not done	Phenytoin, Divalproex
M	28	17	Cryptogenic epilepsy	Scalp EEG: Multifocal spikes and generalized spike waves	Normal	Divalproex, Lamotrigine
M	45	27	Cryptogenic epilepsy	Scalp EEG: Right temporal spikes, seizures	Normal	None

Sex	Age	Onset	Diagnosis	EEG	MRI	Medication
F	41	5	Cryptogenic epilepsy	Scalp EEG: Bifrontal spike waves, maximum right frontal seizures	Normal	Lamotrigine, Divalproex
M	20	12	Idiopathic epilepsy	Scalp EEG: Bifrontal spike waves, maximum right frontal seizures	Normal	Topirimate, Lamotrigine, Lacosamide
F	29	13	Symptomatic epilepsy	Scalp EEG: Right mid-temporal, posterior temporal, right central spikes. Non-localized seizures in right hemisphere.	Right cingulate lesion, dysembryoplastic neuroepithelial tumor; also right temporal periventricular heterotopia	Lamotrigine, Divalproex
F	28	17	--	Scalp EEG: Right mid-temporal ictal discharges, bitemporal interictal spiking	Right mesial temporal sclerosis, asymmetry in the right insular cortex	Levetiracetam, Topiramate
F	32	27	--	Scalp EEG: Left temporal ictal discharges, sporadic left temporal spikes and sharp waves	Focal cortical dysplasia lateral to left genu of corpus callosum; asymmetry in medulla, mid-brain and pons	Lamotrigine
M	27	7	--	Scalp EEG: Left hemisphere ictal onset	Left mesial temporal sclerosis	None

2.2 Experimental Design

MEG and fMRI data were collected in two separate sessions on the same day. In both MEG and fMRI, participants performed a short-term memory task with namable and un-namable visual stimuli. The design of the experiment was identical between MEG and fMRI scanning, with the exception that the timing of trials differed to accommodate the constraints of each imaging modality. Figure 3 provides an overview of the task. Half the trials involved namable items, while the other half involved scrambled, unidentifiable versions of these items. Scrambled items were rearranged at random on a 9 x 9 grid, equally subdivided across the horizontal and vertical axes of the stimuli.

Trials consisted of three phases. First was an encoding phase, in which three images were shown sequentially for 1 s each. Participants were instructed to recite the names of stimuli during a subsequent rehearsal phase of variable length (3–4 s in MEG; 6–12 s for fMRI, selected from a uniform random distribution). For scrambled stimuli, participants were instructed to remember the visual aspects of stimuli instead. Following this, the response phase occurred, in which a probe image was presented that was either novel (50%) or was present during the encoding phase (50%). Participants used their left or right index fingers to respond, indicating whether or not they remembered the probe item from the encoding phase. The assignment of left and right buttons to indicate new or old images was pseudo-randomized and counter-balanced across participants. Participants had 2 s to make a response, and the probe image remained on the screen during this time. In the fMRI study, 25% of the trials did not include the response probe phase. This was

done to facilitate deconvolution of the hemodynamic responses to the rehearsal phase from those of the response phase. Following the response, there was a variable delay of 4–5 s in the MEG experiment and 7–13 s in the fMRI experiment. A total of 128 trials were presented over four sessions of equal length during the MEG scan. This number was reduced to 64 trials over four sessions of equal length during fMRI to account for the increase in trial length.

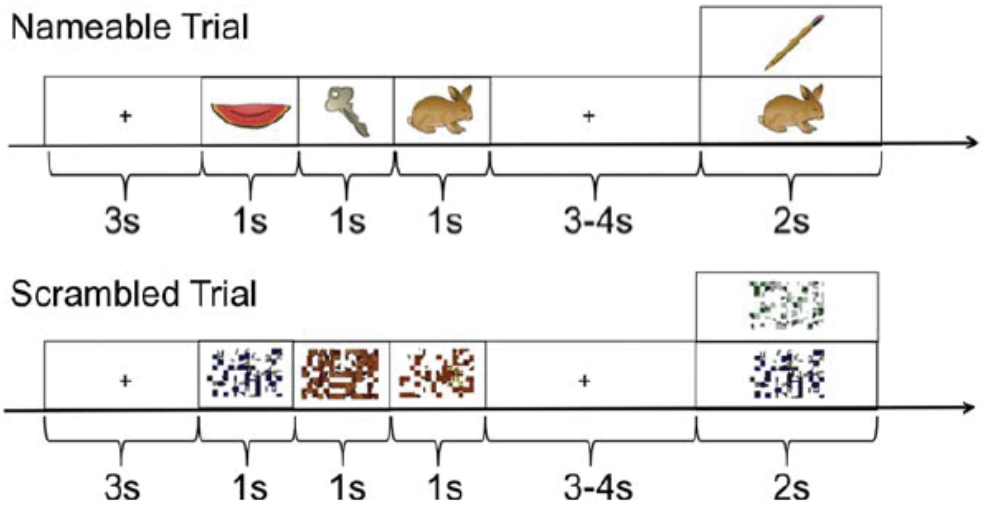

Figure 3 Overview of the working-memory task. Timing refers to the MEG version of the task. Timing for the fMRI version of the task is outlined above.

2.3 Data Acquisition

All MRI data were acquired on a 1.5 tesla GE MRI (GE Medical Systems, Waukesha, WI) at the IWK Health Centre. A 3D T1-weighted anatomical image was acquired using a spoiled gradient recalled (SPGR) sequence (inversion time (TI) = 400 ms, recovery time (TR) = echo time (TE) = min, flip angle = 12 degrees, field of view (FOV) 25.6 cm, 256 x 256, 2 mm thick slices). Functional MRI data were

acquired using a spiral out sequence (TR = 2.2 s, TE = 40 ms, flip angle = 90 degrees, 24 cm FOV, 64 x 64, 4.5 mm thick slices).

MEG data were acquired using a 306 channel whole-head Elekta Neuromag MEG system (Elekta Neuromag, Helsinki, Finland). The system was located in a magnetically shielded room and was equipped with 102 magnetometers and 204 planar gradiometers. A separate MEG scan was performed for each of four sessions of the experimental paradigm. MEG data were acquired at a sampling rate of 1000 Hz. Head position was monitored using four electromagnetic head position indicator (HPI) coils. The position of these coils was tracked in relation to the nasion and left and right preauricular points, all of which were digitized using a 3D position monitoring system prior to scanning (Polhemus, Colchester, VT). In addition, approximately 150 points on the surface of the scalp were recorded for co-registration with anatomical MRI data.

2.4 Behavioral Analysis

Trials were subdivided into four conditions (nameable-old, nameable-new, scrambled-old, scrambled-new). Response time and response accuracy were recorded for each trial. To account for the bimodal distribution of response accuracy (correct vs. incorrect), its log-odds were modeled (Dixon, 2008) as a function of fixed effects (imaging modality, stimulus type, probe novelty, trial number, and participant group), with participant modeled as a random effect using the 'lme4' package (Bates, Maechler, & Bolker, 2011) in R (R Development Core Team, 2008). To find evidence for interactions, the Akaike Information Criterion (AIC; Akaike,

1974) was calculated for a model including the highest-order interactions, and for a model with no interactions. Contrasting AIC values indicated the degree to which the model was improved by inclusion of the interactions. Inclusion of interactions was thresholded at an AIC contrast of 5.0, and models were iteratively compared until all lowest-order interactions were evaluated as necessary. Subsequently, raw response time was modeled as a function of the same effects using this procedure. Iterative model fitting and post-hoc testing of interactions were performed using the 'LMERConvenienceFunctions' R package (Tremblay & Ransijn, 2013).

2.4 fMRI Analysis

Analysis of fMRI data was performed using fMRI Expert Analysis Tool (FEAT) version 5.98 (Smith et al., 2004), a part of FMRIB's Software Library (FSL). For three control participants and two people with epilepsy, one of the four sessions was excluded due to file corruption. One additional person with epilepsy did not respond during one session, resulting in its exclusion. Pre-statistical analyses included skull removal using FSL's Brain Extraction Tool (BET; Smith, 2002), motion correction using MCFLIRT (Jenkinson, Bannister, Brady, & Smith, 2002), spatial smoothing with a FWHM of 5 mm, and application of a 0.01 Hz high pass filter. No scans were excluded due to excessive motion. Prewhitening and statistical analysis were completed using FMRIB's Improved Linear Model (FILM) with local autocorrelation correction (Woolrich, Ripley, Brady, & Smith, 2001). Functional data were analyzed for presence of activity using the general linear model in FEAT. Stimulus onset vectors were convolved with the double gamma HRF for the encoding phase and for

probe items separately. Motion covariates generated during motion correction were included as model parameters of no interest.

Activation associated with the two types of encoding stimuli (nameable and scrambled) was contrasted. Activation maps were thresholded at z = 2.3 with a minimum cluster size of 250 voxels on a 1 mm isotropic grid. Functional data were registered to a T_1 weighted anatomical image of the participant's brain at 6 degrees of freedom (DOF). Anatomical and functional MRI data were subsequently normalized using FMRIB's Linear Registration Tool (FLIRT; Jenkinson et al., 2002) to the template defined by Talairach & Tournoux (1988). The same stimulus contrast was performed at the group-level using a mixed effects model, as implemented by FLAME (FMRIB's Local Analysis of Mixed Effects), a part of FSL.

2.5 MEG Analysis

Environmental noise was reduced using temporal signal-space separation (Taulu, Kajola, & Simola, 2004). MEG scans were excluded if intrascan movement of any HPI coil exceeded 1 cm for a participant. Data were downsampled to 125 Hz. Within a trial, the time window of interest (200-600ms following stimulus presentation) for each of the three encoding images was averaged together, resulting in one 400 ms epoch per trial. This time range was selected to capture source activity of the highest amplitude, as identified in a previous analysis of these data (D'Arcy et al., 2013). Similarly, three non-overlapping time windows of equal length (i.e., 400 ms) from the 1200 ms immediately prior to presentation of the first image of each trial were averaged to form a baseline. Principal components of MEG epochs that exceed 1.0 pT in strength (magnetometers) or 150 fT/cm^2

(gradiometers) were removed as artifacts (Kobayashi & Kuriki, 1999; Lagerlund, Shardbrough, & Busacker, 1997). For people with epilepsy, trials containing interictal activity were rejected based on visual inspection.

Trials were categorized as either nameable or scrambled depending on stimulus type. Trials were averaged, resulting in activation and baseline periods for each of the two stimulus types. A signal space separation beamformer was used to generate whole-brain activation maps for each using a 0.1 – 40 Hz waveband (Vrba et al., 2010). Maps were calculated on a 4 mm isotropic grid. Spatiotemporal activation maps were collapsed over time for each voxel individually. For a voxel, activity within a 48 ms window surrounding the time point of highest intensity was averaged. This calculation was performed iteratively across the brain, resulting in a single three-dimensional map showing clusters of activity from early or late times in the active window.

Maps were normalized spatially by a Talairach transformation, implemented using AFNI version 2011-12-21-1014 (Cox, 1996). Group activation was calculated using voxel-wise linear mixed effects modeling with the lme4 package (Bates et al., 2011) in R (R Development Core Team, 2008). Fixed effects (stimulus type) and random effects (participant, stimulus type by participant) modulated voxel intensity. Activation maps were thresholded at $p < .01$ with a minimum cluster size of 250 voxels on a 1 mm isotropic grid.

2.6 MEG-fMRI Integration

In order to determine the degree of influence from each map over the integrated map, the contrast-to-noise ratio (CNR) was calculated for every voxel.

This measure was chosen over the commonly used signal-to-noise ratio (SNR) to be more representative of the final nameable vs. scrambled stimulus contrast activity. For fMRI, contrast was the mean difference between parameter estimates for nameable vs. scrambled images across participants. For MEG, contrast was the mean difference between beamformer pseudo *z* scores for the two stimulus types for a voxel. For each, noise was defined as the variance in the contrast. This method of CNR calculation has been successfully applied to fMRI data in the past as a data quality parameter (Geissler et al., 2007). This ratio is reminiscent of statistical hypotheses testing methods, with the primary differentiating factor being incorporation of degrees of freedom in hypothesis testing. These calculations were performed on temporally and spatially filtered fMRI data, and on localized MEG data, which has an inherent degree of smoothing. The CNR was then used to calculate a weighted average for each voxel when integrating the MEG and fMRI activation t-maps. This is shown in Formula 1, where the integrated activation value for a voxel (I) is the sum over every i, where i is the imaging modality, W is the CNR weight, and A is the activation value. The integration method applied here can be expanded to include any number of different types of activation maps, requiring only an equivalent weighting factor and voxel intensity. Activation maps were thresholded at $p < .01$ with a minimum cluster size of 250 voxels on a 1 mm isotropic grid.

$$I = \frac{\sum(W_i \times A_i)}{\sum W_i} \quad (1)$$

2.7 Laterality Mapping

Following integration, a Complex Laterality Vector (CLV) was calculated for each significantly active voxel by pairing spatially homologous voxels between the left and right hemispheres in the spatially normalized brain. Our lab has previously demonstrated the creation of the CLV using MEG data localized to the cortical surface (D'Arcy et al., 2013). The CLV is a two-dimensional construct that contains the magnitude of activity in spatially homologous pairs of voxels in the left and right hemispheres. This vector is represented as a complex number, containing one real component (left hemisphere activity) and one imaginary component (right hemisphere activity), as seen in Formula 2. The real component is the intensity of any voxel from the left hemisphere (Q_{lh}). The imaginary component is created by multiplying the intensity of that voxel's right-hemisphere homologue (Q_{rh}) by the mathematical constant *i* which represents the square root of negative one. This calculation was performed for each pair of voxels in the brain.

$$CLV = Q_{lh} + i \times Q_{rh} \quad (2)$$

The CLV was visualized by plotting left-only and bilateral activation on the left hemisphere. Right-only and bilateral activation were plotted on the right hemisphere. Left-only, right-only and bilateral voxels were defined based on the presence of significant activity in their homologue in the opposing hemisphere. The real component (Q_{lh}) was plotted using a red-to-yellow color scale. The imaginary component (Q_{rh}) was plotted using a blue-to-cyan color scale. Bilateral regions were

plotted using a sum of these color scales (purple-to-white) where relevant, depicting both the magnitude of activity in each hemisphere and the degree of laterality using a single two-dimensional scale.

3 Results

3.1 Behavioral Measures

All reaction time and response accuracy effects are depicted in Table 2. Response accuracy showed a significant main effect for stimulus type (nameable > scrambled, $p < .001$). There was a significant interaction between imaging modality and probe novelty ($p = .002$), such that accuracy for novel probe items was significantly higher than for those previously seen for the MEG version of the task ($p < .001$), but not the fMRI version. Similarly, response time showed a significant main effect of stimulus type (scrambled > nameable, $p < .001$). Additional main effects were found for imaging modality (fMRI > MEG, $p < .001$), and trial number ($p < .001$). A significant interaction was found between participant group and imaging modality ($p = .002$). While there was a trend toward a larger group difference in response times for the MEG version of the task than for fMRI, neither of these differences were significant.

Table 2 Response accuracy and time for trials with responses in both the MEG and fMRI versions of the task, with significant effects and interactions.

Accuracy	n	Probability (%)	Standard Error	*z*	*p*
Type	3377	Nameable: 97.88 Scrambled: 77.84	Nameable: 0.37 Scrambled: 3.41	13.05	< .001
Modality * Novelty	3377			3.06	0.002
Response Time	DOF	Estimate (ms)	Standard Error	*F*	*p*
Type	1, 3348	Nameable: 974 Scrambled: 1158	Nameable: 70 Scrambled: 61	372.79	< .001
Modality	1, 3348	MEG: 878 fMRI: 1158	MEG: 79 fMRI: 61	345.34	< .001
Trial	1, 3348	0.48	0.14	11.53	< .001
Group * Modality	1, 3348			9.48	0.002

3.2 Functional MRI

Group activation for healthy control participants showed prominent clusters in both hemispheres. Left-lateralized activation was noted in the inferior prefrontal cortex, inferior parietal cortex, insula, hippocampus and parahippocampal gyrus. Significant bilateral activation was found in lateral and medial occipital lobes, anterior prefrontal cortex and the fusiform gyrus.

People with epilepsy showed a more widespread and bilaterally distributed pattern of activation than was seen in control participants. Left-lateralized clusters were localized to inferior prefrontal cortex, insula, superior temporal sulcus and supramarginal gyrus. Remaining activation in temporal and occipital regions was

bilaterally distributed, including clusters in lateral and medial occipital cortices, fusiform gyrus, inferior parietal lobe and parahippocampal gyrus. Activation for the two groups is shown in Figure 4.

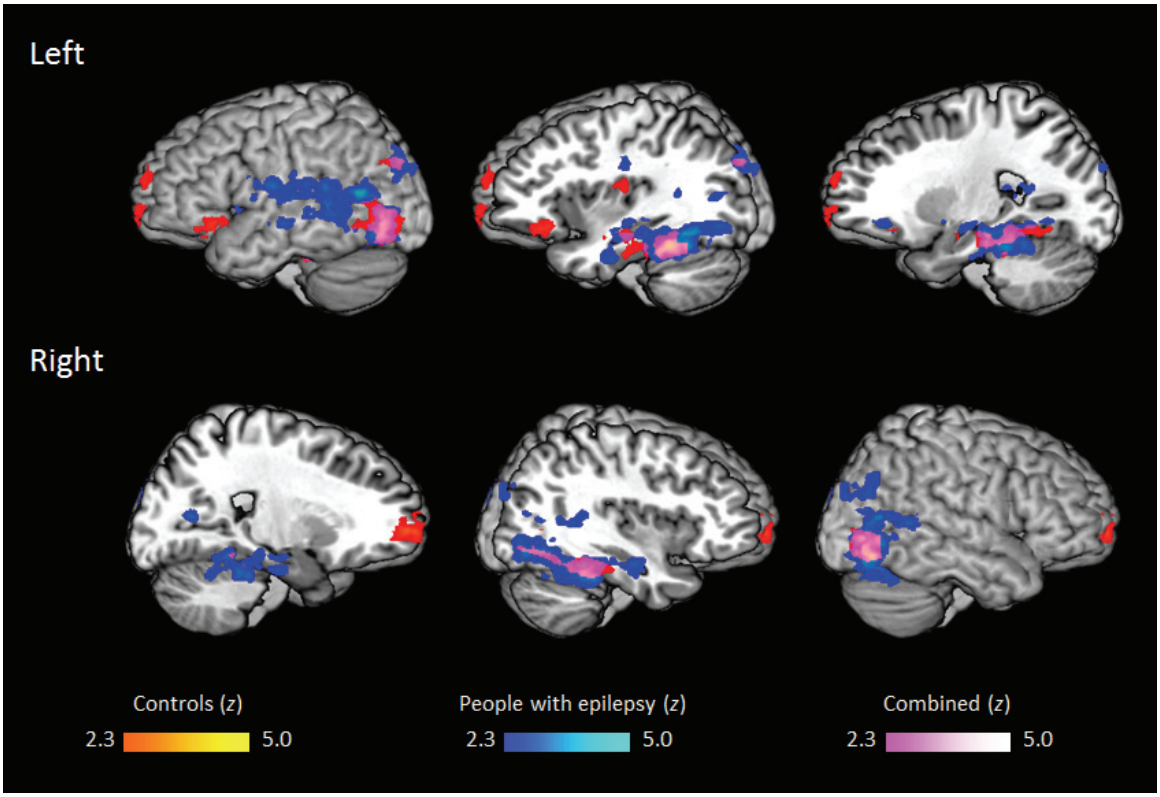

Figure 4 Functional MRI activation for healthy control participants (red) and people with epilepsy (blue). The nameable vs. scrambled stimulus contrast is shown. The sums of common areas of activation are shown in purple. Activation is thresholded at $z = 2.3$, with a minimum cluster size of 250 voxels.

3.3 MEG

MEG data for healthy controls were localized to fewer regions than were found using functional MRI. In the left hemisphere, clusters were found in the temporal pole, parahippocampal gyrus and lateral occipital cortex. Significant activation was also found in the inferior parietal lobe of the right hemisphere. Active clusters were localized in the frontal poles of both hemispheres. Data for people with epilepsy were localized to the anterior inferior temporal gyrus of the left hemisphere, with additional right-hemisphere activity found in the insular cortex and throughout the medial wall of the superior frontal gyrus, including the supplementary motor area (SMA). Activation maps for the two groups are shown in Figure 5.

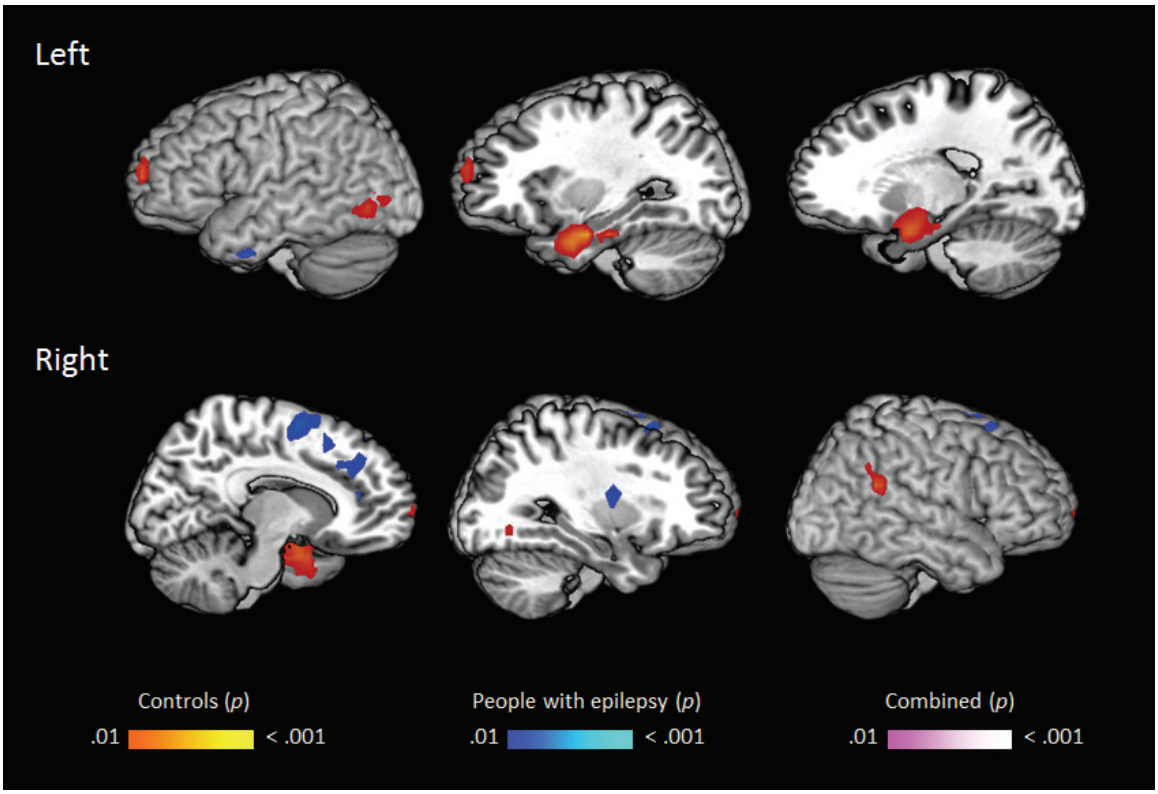

Figure 5 MEG activation for healthy control participants (red) and people with epilepsy (blue). The nameable vs. scrambled stimulus contrast is shown. Activity is collapsed across time, showing both early- and late-occurring clusters. The sums of common areas of activation are shown in purple. Activation is thresholded at $p < .01$, with a minimum cluster size of 250 voxels.

The time courses for significantly active clusters can be seen in Figure 6. The peaks of time courses in control participants showed propagation of signal from lateral occipital cortex (260 ms) to anterior portions of the temporal lobe (530 ms) following stimulus presentation. Transient activity was seen in the right inferior parietal cortex, with local peaks at 230 ms and 430 ms. The time courses for people with epilepsy are also shown. The anterior portion of the inferior temporal gyrus, located laterally to temporal lobe activity found in healthy controls, demonstrated similar early activity (240-280 ms). However, later anterior temporal activity found

in controls was not present in people with epilepsy. Activity was found in the right superior frontal gyrus occurring early (200-300 ms), with its strongest activity occurring later at 440 ms.

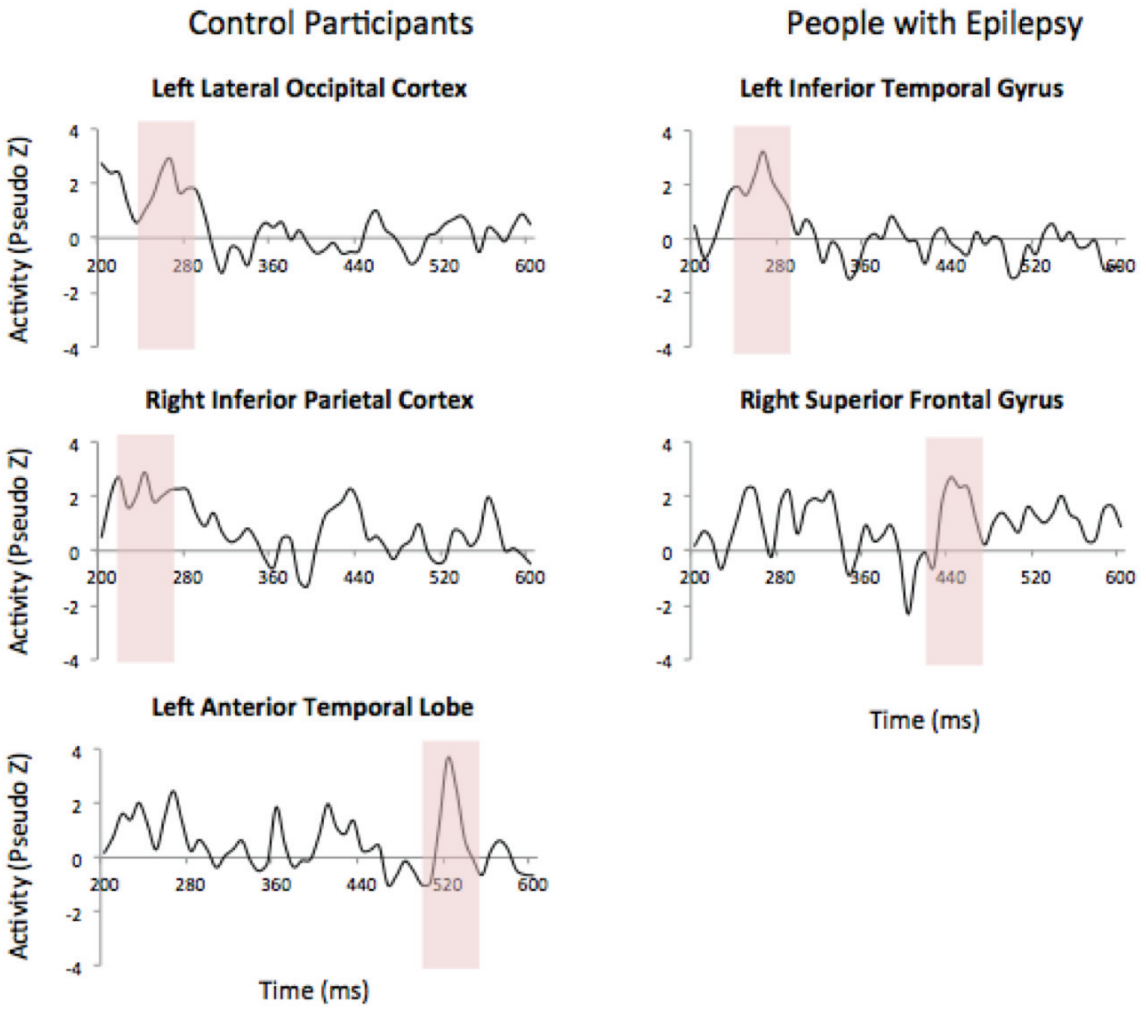

Figure 6 Time courses for presentation of nameable objects contrasted with scrambled images. Pseudo z activation values are averaged across the voxels of significantly active clusters at every time point in controls and people with epilepsy. Red regions depict the 48ms window used for activation maps.

3.4 Integrated MEG-fMRI

Integrated MEG-fMRI activation maps were calculated by weighting the two data sets by their respective CNR at each voxel. For healthy control participants, left-lateralized activation was found in the inferior prefrontal cortex, parahippocampal gyrus and hippocampus, and in the superior parietal lobule. Right-lateralized clusters were located in the inferior parietal lobe and supramarginal gyrus. All other clusters were bilaterally distributed in the fusiform gyrus, lateral and medial occipital cortex, and anterior prefrontal cortex and frontal poles.

Consistent with what was observed from fMRI-only analyses, people with epilepsy demonstrated a more widespread and bilaterally distributed set of active regions in response to the task. Left-lateralized clusters were found in the inferior prefrontal cortex, superior and inferior temporal gyrus, and superior parietal lobule. Right-lateralized clusters were located in the inferior parietal lobe. Remaining clusters were bilaterally distributed across the superior frontal gyrus, medial and lateral occipital cortex, fusiform gyrus, hippocampus and parahippocampal gyrus. Activation maps for the two groups are shown in Figure 7.

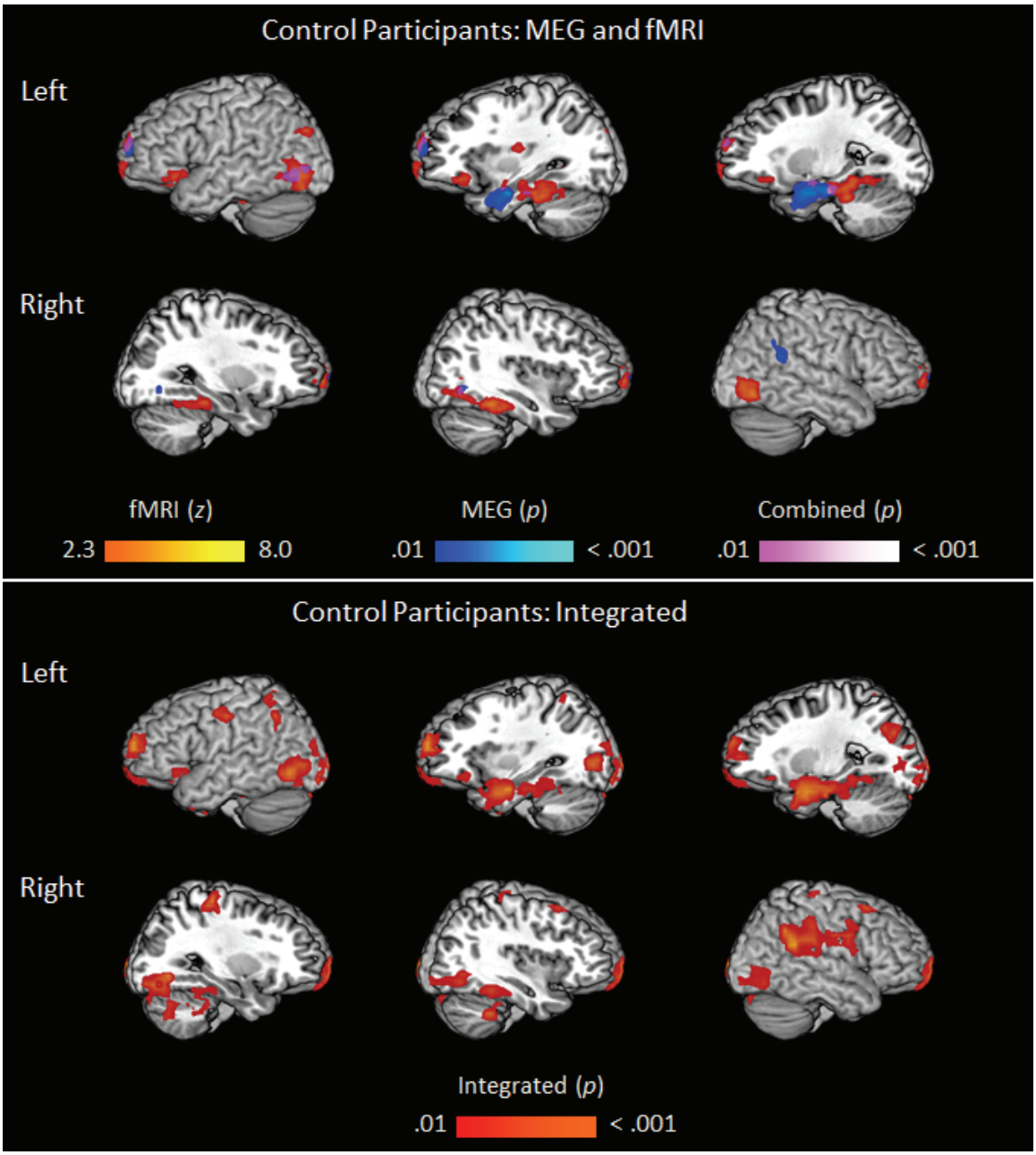

Figure 7 Overlaid MEG and fMRI activation for control participants (top), and their integrated activation (bottom). Activation is thresholded at $p < .01$ (MEG and integrated) and $z > 2.3$ (fMRI), with a minimum cluster size of 250 voxels.

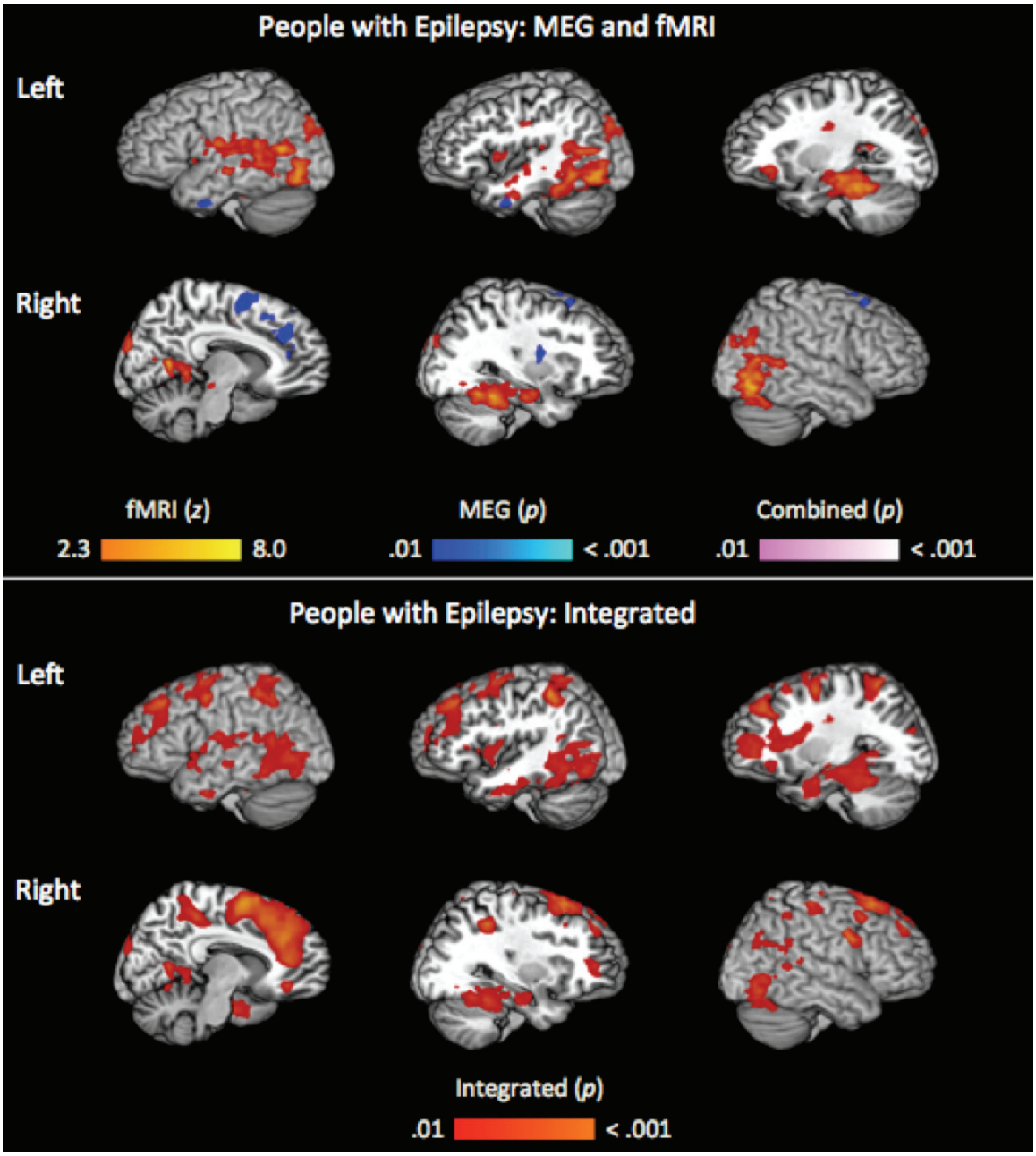

Figure 8 Overlaid MEG and fMRI activation for people with epilepsy (top), and their integrated activation (bottom). Activation is thresholded at $p < .01$ (MEG and integrated) and $z > 2.3$ (fMRI), with a minimum cluster size of 250 voxels.

3.5 MEG & fMRI Sensitivity Profiles

As discussed, a primary intention of the present study was to determine whether we could compensate for signal loss in anterior temporal regions (where magnetic susceptibility artifact can distort fMRI signal) and subcortical gray matter regions (where magnetic field loss with distance renders MEG less sensitive) by using multimodal neuroimaging. In order to determine the relative sensitivity of MEG and fMRI to activity in these and other regions, the contrast-to-noise ratios for both were plotted and contrasted across the brain for the control group. The contrasted CNR map is shown in Figure 9, representing the relative sensitivity profiles of the two imaging modalities and the weighting of their activation maps during integration.

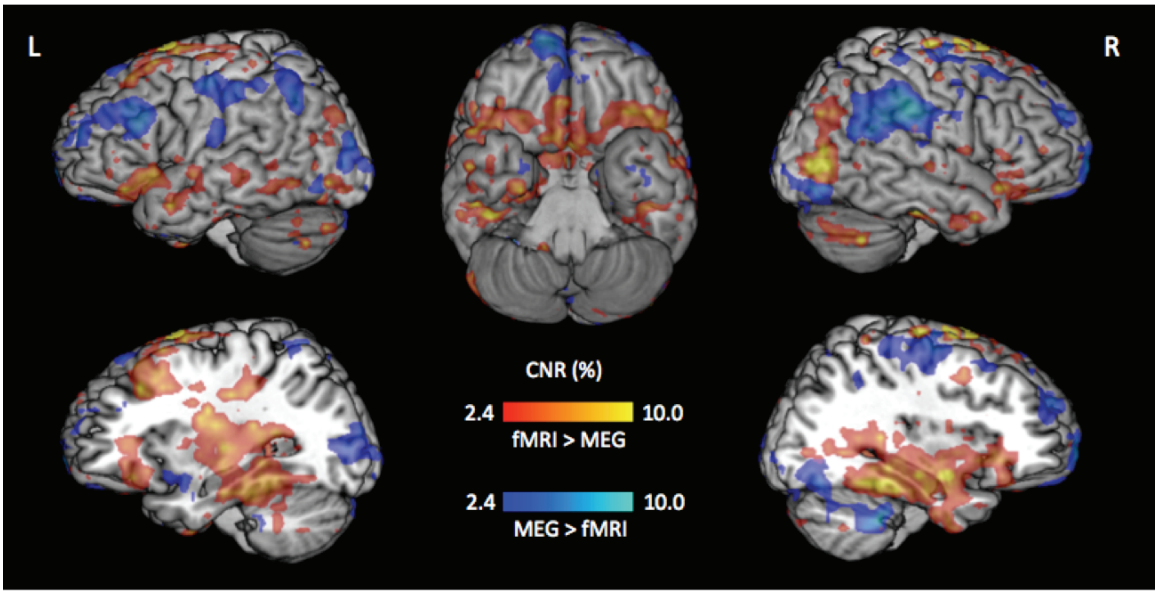

Figure 9 Contrasted MEG vs. fMRI CNR plotted across the brain, depicting regions in which sensitivity is higher for fMRI (red) and for MEG (blue). The CNR map reflects the weighting of the two data sets in each region during integration.

While MEG showed increased sensitivity over fMRI in localized portions of the frontal poles, the CNR contrast did not suggest that either modality was predominantly sensitive to activity in the anterior temporal lobes. Additional regions that demonstrated preferential MEG sensitivity included extensive portions of the middle frontal gyrus and inferior parietal cortex, as well as posterior occipital cortex. Sensitivity was shown to be higher for fMRI than for MEG throughout the lateral and medial temporal lobes, including the hippocampus bilaterally, as well as the inferior frontal gyrus and superior frontal gyrus.

The effect of applying the CNR weights to the integrated activation maps can be seen in Figure 10. The integrated MEG-fMRI activation map was calculated for control participants both with and without application of the weighting method described above. When integrated without the CNR weights, a reduced subset of regions was shown to be active: left-hemisphere activation was only found in the lateral occipital cortex, frontal pole and parahippocampal gyrus. No activation was present in the right hemisphere. Integration of MEG and fMRI activation maps without weighting was shown to result in reduced sensitivity to regions across the brain.

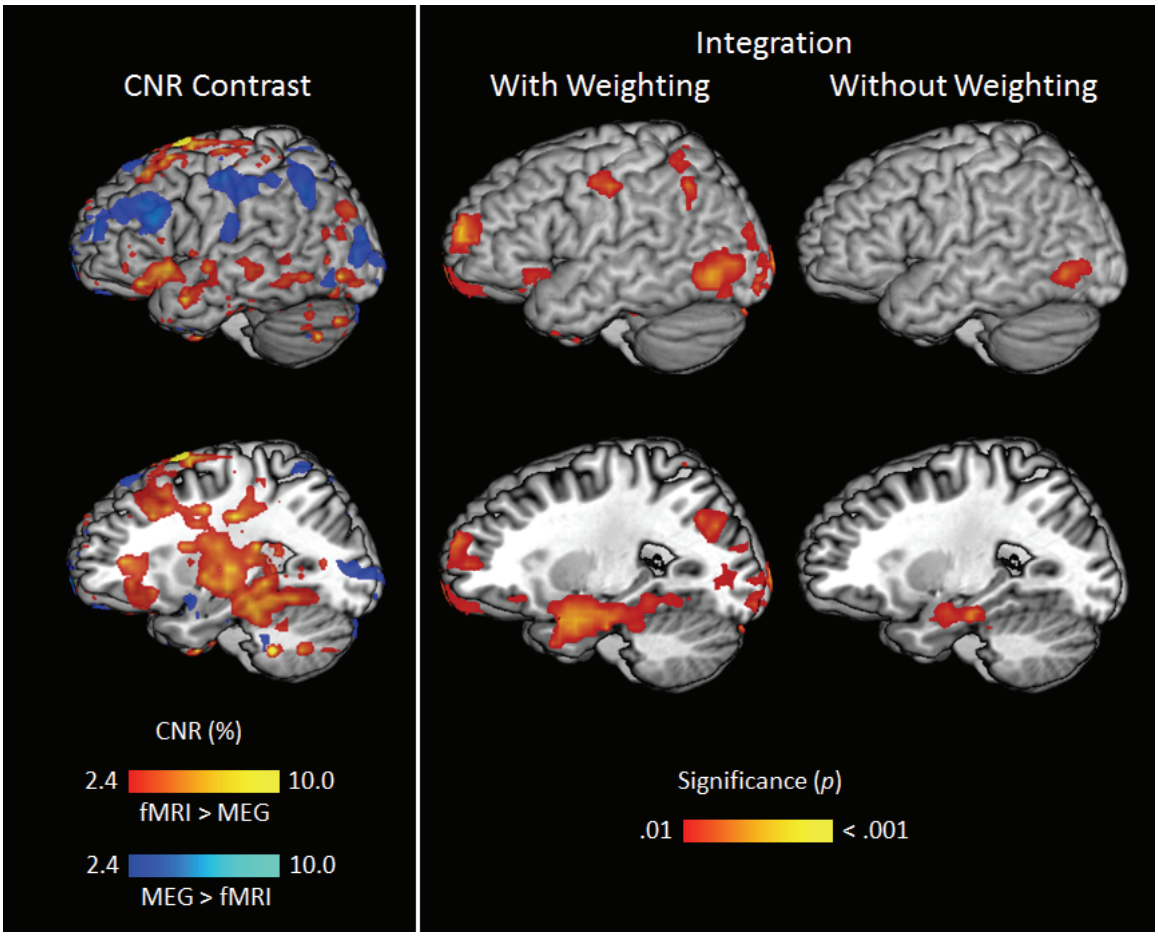

Figure 10 Contrasted MEG and fMRI CNR alongside integrated MEG-fMRI activation for healthy control participants, combined with CNR weights (left) and with equal weight (right). Activation was thresholded at $p < .01$ with a minimum cluster size of 250 voxels.

3.6 Laterality Mapping

Laterality maps were calculated for the control participants and for people with epilepsy using the integrated MEG-fMRI activation maps. Laterality of activity for the control group is shown in Figure 11. Bilateral activation was most prominent in the fusiform gyrus and lateral occipital cortex, as predicted, as well as the anterior prefrontal cortex. Hippocampal and parahippocampal activation showed left lateralization, along with inferior prefrontal cortex and a large portion of medial

occipital cortex. While activation in the frontal poles was present in both hemispheres, only activity on the medial wall was shown to be bilateral. Right-lateralized activation was limited to portions of the parahippocampal gyrus and the inferior parietal lobe.

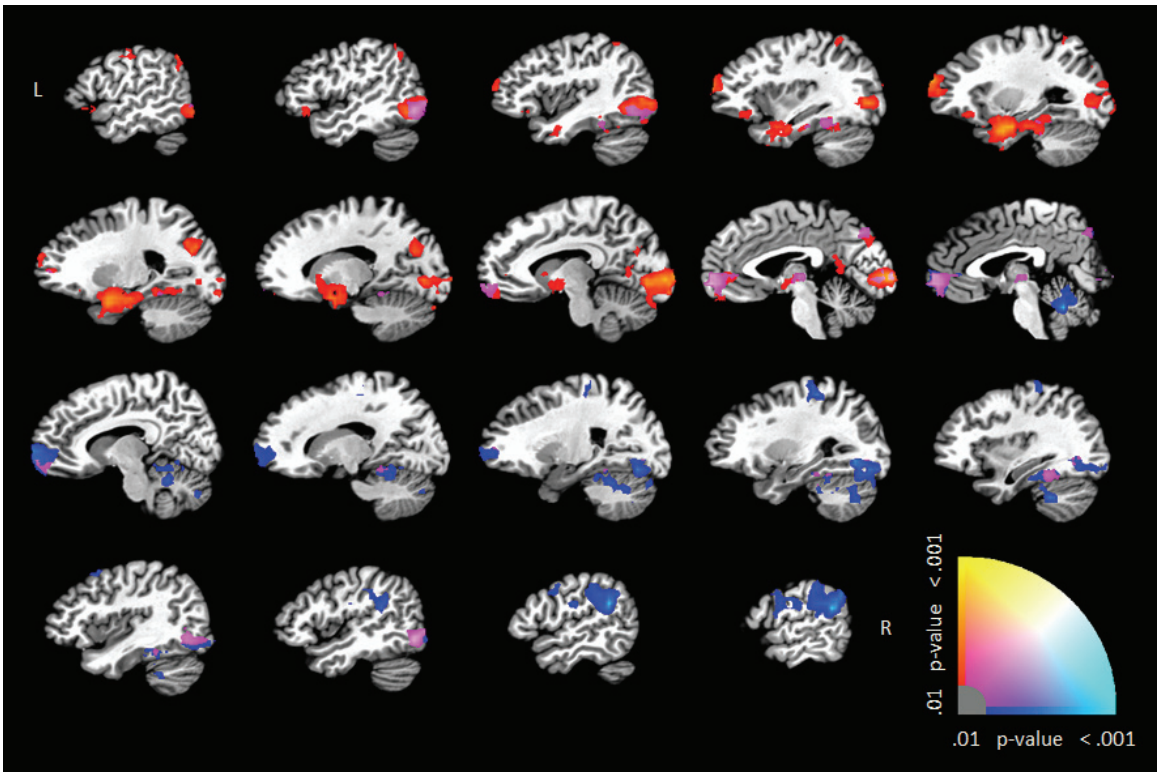

Figure 11 Laterality map of integrated MEG-fMRI activation for healthy control participants. Activation in the left hemisphere is plotted in red-to-yellow (left), blue-to-cyan (right), and purple-to-white (bilateral). Activation was thresholded at $p < .01$.

The CLV maps confirmed our earlier qualitative observations that people with epilepsy showed increased bilateral dominance and a more widespread distribution of active regions across the two hemispheres. Figure 12 depicts bilateral activation in the lateral occipital cortex, and extensively in the medial temporal lobe through the fusiform gyrus, hippocampus and parahippocampal

gyrus. While bilateral activity was present in the anterior hippocampus, additional activity in posterior portions was left-lateralized. Activation in the lateral temporal cortex also demonstrated left-hemisphere lateralization, including clusters in the superior and middle temporal gyrus. Dorsal and medial portions of the superior frontal gyrus showed right-hemisphere lateralization with bilateral regions on the medial wall, extending to the anterior cingulate gyrus. Inferior parietal clusters were also seen in the right hemisphere, with partial bilateral dominance.

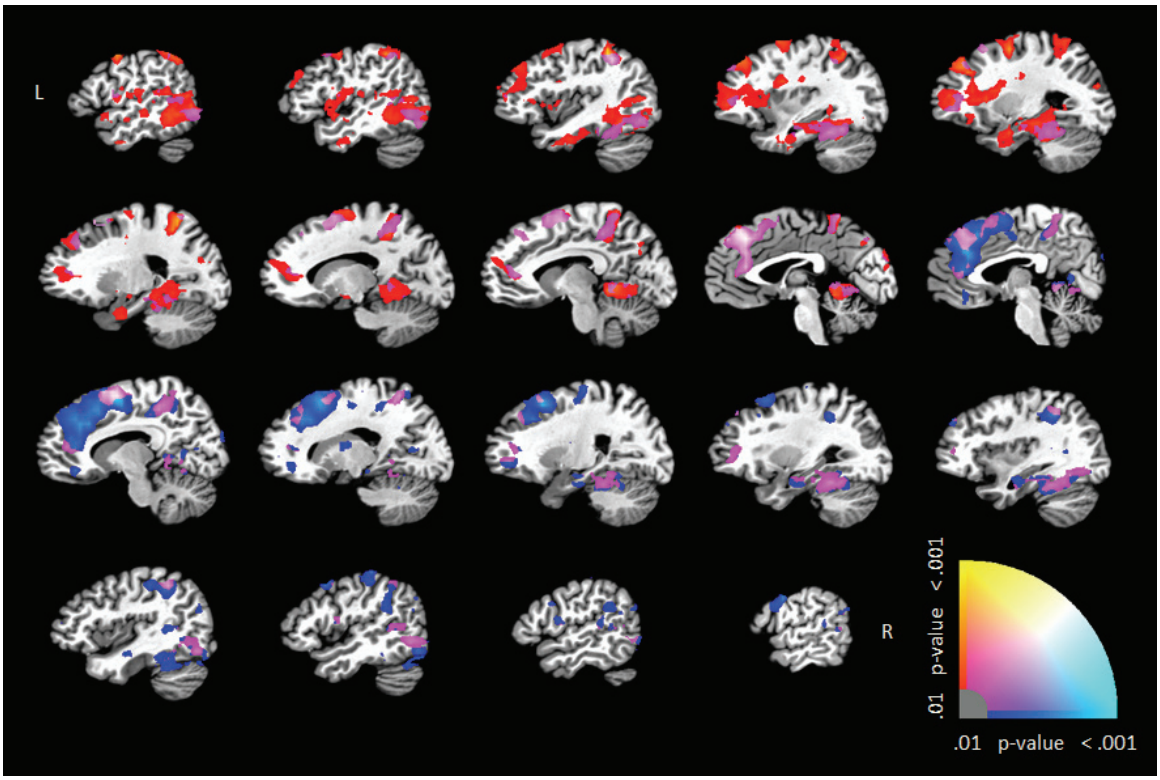

Figure 12 Laterality map of integrated MEG-fMRI activation for people with epilepsy. Activation in the left hemisphere is plotted in red-to-yellow (left), blue-to-cyan (right), and purple-to-white (bilateral). Activation was thresholded at $p < .01$.

3.7 Regional Laterality

The laterality of various regions activated by the task was assessed using traditional laterality indices, as well as complex laterality vectors, for both people with epilepsy and control participants. This was done for each region for which we had specified a hypothesis a priori: the fusiform gyrus, parahippocampal gyrus up to the most anterior portion of the hippocampus, the hippocampus, inferior frontal gyrus, and temporal lobes anterior to the hippocampus. The results can be seen in Figure 13. Our previously established cutoff for the laterality index was used to indicate left (values above 0.1) or right (values below -0.1) hemispheric dominance (D'Arcy et al., 2013), where values between the two indicated bilateral dominance. Left and right hemisphere activity were subsequently investigated using complex laterality vectors for these regions in order to indicate either weak or strong activity for each hemisphere, as this information was not apparent using the laterality index.

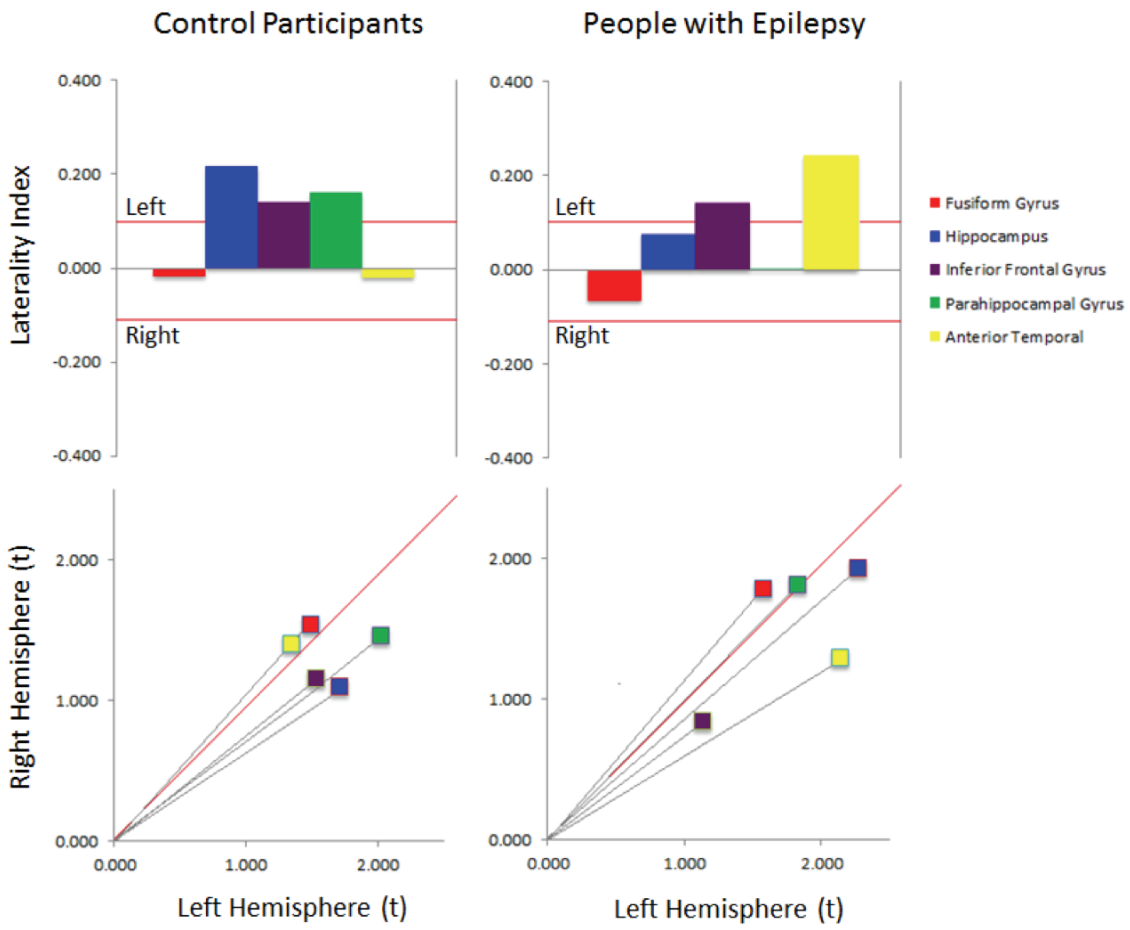

Figure 13 LI (top) and CLV (bottom) for regions that showed activation in the integrated MEG-fMRI map. Positive LIs and CLVs below 45° indicated left lateralization, while negative LIs and CLVs above 45° showed right lateralization.

The healthy control group showed a predominantly left-lateralized network of activation by both LI and CLV methods, including the hippocampus, parahippocampal gyrus and inferior frontal gyrus. For control participants, activity in the fusiform gyrus and anterior temporal lobes was more bilaterally distributed, as indicated using both methods. While the parahippocampal gyrus and inferior frontal gyrus both had LI scores indicating similar degrees of left-lateralization, their CLVs showed relatively stronger activation in the parahippocampal gyrus.

Additionally, while the fusiform gyrus and anterior temporal lobes showed nearly identical LIs, the activity in the fusiform gyrus was stronger than in the anterior temporal lobes, as made apparent only by their CLVs.

Using both LI and CLV methods showed that while people with epilepsy had similar left-hemisphere lateralization in the inferior temporal lobes, bilateral activity was found in the hippocampus and parahippocampal gyrus. In addition, both methods showed left-hemisphere dominance for activity in the anterior temporal lobes, as opposed to the bilateral pattern found in control participants. Bilateral activation was also noted in the fusiform gyrus using both methods. It should be noted that while the LI for the inferior frontal gyrus was strong in relation to other regions, its CLV indicated that activity was weakest of all regions. Furthermore, the LI for the hippocampus showed bilateral dominance. The CLV for this region further demonstrated strong bilateral activity, as opposed to weak. This information is critical as both scenarios result in an equivalent LI but indicate varying degrees of functioning.

4 Discussion

The present study aimed to improve on available laterality assessments for presurgical evaluation in two ways: 1) By using multimodal neuroimaging to find activity in low-sensitivity regions, and 2) by calculating high-resolution maps of laterality. Both of these steps represent critical advances in laterality assessment, as current assessments are either non-specific to regions within a hemisphere and instead represent larger-scale hemispheric dominance, or rely solely on fMRI and are therefore susceptible to loss of sensitivity in the commonly resected anterior temporal lobe.

All hypotheses were confirmed by the results of the study. First, it was predicted that activity would be localized to regions involved in verbal memory processing and object identification, as consistent with previous research (Bar et al., 2001; Bellgowan et al., 2009; Grill-Spector et al., 2001). This strengthens the assessment as a useful clinical tool for presurgical evaluation. Additionally, it was hypothesized that MEG would show relatively greater sensitivity than fMRI in anterior temporal lobes, while fMRI would show greater sensitivity in the hippocampus. Both of these regions are of clinical interest, and each poses difficulty to one modality. Finally, it was predicted that the integrated MEG-fMRI activation map would show activity in both of these regions, where each modality alone would only show activity in one. Taken together, these findings suggest that the present laterality assessment shows enhanced sensitivity to a range of regions considered during presurgical evaluation.

4.1 Behavioral Validation

Participants in both groups demonstrated understanding of the task. Regarding both accuracy and response time, a significant main effect was seen for stimulus type, but not for probe item novelty. Because novelty was not a contrast implemented in the present analysis, these findings suggest that the activation seen was the result of the stimulus type contrast, and was therefore reflective of verbal encoding and object identification processing. Additionally, there was a significant main effect for modality in response time, showing faster responses for the MEG version of the task. This difference in response times occurred irrespective of accuracy. This difference can likely be attributed to the change in timing that was necessary to accommodate the two modalities. While the rehearsal phase for the MEG version of the task was 3 – 4 s in length, this was increased to 6 – 12 s in the fMRI version. This increase may have necessitated more extensive reflection on probe items, decreasing speed but not accuracy. This difference may have also accounted for the interaction between imaging modality and probe novelty in response accuracy, such that increased rehearsal phase time may lead to uncertainty regarding probe item novelty.

Interestingly, an interaction was present between probe novelty and imaging modality for accuracy, such that a notable difference was seen between old and new items for the MEG version of the task, but not for fMRI. As with response time differences, this can likely be attributed to modification of rehearsal phase duration, reducing the saliency of new relative to old stimuli with time. Additionally, the trend toward slower responses for people with epilepsy was considerably stronger for the

MEG version of the task than the fMRI version. Interactions including the imaging modality may be party driven by participant fatigue, as fMRI data were recorded in the evening, several hours after MEG data recording. The present data do not allow for clear interpretation of this difference, but the trend may be indicative of group-related differences in processing speed that vary systematically with task demands.

4.2 Neuroanatomical Substrates of the Task

Regions that showed activation aligned with the hypotheses, suggesting that the present task is a valid assessment for verbal encoding and object identification. Control participants showed activation bilaterally in lateral occipital cortex, a primary constituent of the ventral visual stream, which processes the form and representation of objects (Goodale & Milner, 1992). This and additional occipital regions are involved in identification of complex or recognized objects (Grill-Spector et al., 2001).

Both the dorsal and ventral visual streams have connections to the prefrontal cortex (Cavada, Compañy, Tejedor, Cruz-Rizzolo, & Reinoso-Suárez, 2000). Frontal cortical connections have been related to using visual information in decision making and reward processing (Fuster, 1997). This region is also involved in classifying and categorizing objects in relation to past experiences (Schacter, Gilbert, & Wegner, 2011). Therefore, while activation seen in frontal poles is not conventionally associated with language or object processing, it may be the result of preparation for response to probe items, at which time participants were required to determine the novelty of images. In this case, categorization of objects may be a useful strategy for future recall-based decision-making. Importantly, Chouinard,

Whitwell and Goodale (2009) demonstrated the role of the lateral occipital cortex in recognition of visual aspects of objects, and the left inferior frontal gyrus in object naming, using transcranial magnetic stimulation. Activity in both regions in unsurprising given the spatial and verbal requirements of the task.

Several of the active regions have been associated with speech production. Their involvement with the present task may be reflective of this set of functions, as participants were instructed to verbally recite the names of objects. Most notably, this includes activity in the left insular cortex and posterior inferior frontal gyrus for both groups using fMRI. Additionally, MEG activation maps for people with epilepsy demonstrated activity in the supplementary motor area. A meta-analysis of speech production has reliably associated each of these regions with related processes (Indefrey & Levelt, 2004). While activity in the primary motor cortex is typically expected in a speech production paradigm, it should be noted that participants recited object names mentally and thus no explicit motor activity was expected.

Activation seen in the left hippocampus and parahippocampal gyrus, and bilateral fusiform gyri have been shown to process recognized vs. unrecognized objects using fMRI (Bar et al., 2001). These regions are of key clinical concern, and their activation was a goal of the study. These findings align with the demands of the task, reflecting recognition of nameable objects, but not scrambled stimuli. In addition, the hippocampus is known to have involvement in both spatial and verbal memory encoding, and is thought to function as a part of a larger network of regions in the temporal lobe for declarative memory processing (Squire, 1992). Recognition and memory of stimuli is likely to have incorporated both of these sets of processes,

as participants were instructed to mentally verbalize the nameable objects presented to them.

Interestingly, the time courses of activity in anterior temporal regions varied between people with epilepsy and control participants. This may be due to anterior temporal activity being localized laterally to activation seen in control participants. The two regions showed similar activity during early time periods (200 - 300 ms), with subsequent divergence. This group difference may have been the result of minor variation in cluster location between controls and people with epilepsy.

The complex laterality vector and laterality index for anterior temporal lobes depicted a more left-lateralized network of activity for people with epilepsy than for control participants, who showed bilateral dominance using a conventional laterality score cutoff. Figure 6 demonstrates that the left-lateralized activity seen for people with epilepsy is occurring between 200 ms and 300 ms following stimulus onset. Finally, activation in the dorsomedial area of the occipital lobe included the lingual gyrus, which is known to facilitate connection between primary visual processing regions the limbic system (Bogousslavsky, Miklossy, Deruaz, Assal, & Regli, 1987). The lingual gyrus is also involved in processing of verbal information, and the naming of visual stimuli (Bookheimer, Zeffiro, Blaxton, Gaillard, & Theodore, 1995). Taken together, these data suggest that the demands of the task were representative of functions commonly assessed prior to surgery, including confrontation naming and verbal working memory.

4.3 Sensitivity of MEG and fMRI

The contrasted CNR profiles of MEG and fMRI and their respective activation maps supported the hypothesis regarding sensitivity to hippocampal and anterior temporal lobe activity. The CNR contrast suggested that fMRI has greater sensitivity to activity throughout the medial and lateral temporal lobes, including the hippocampus and parahippocampal gyrus. This is reflected in activation maps, showing fMRI but not MEG activity in the hippocampus. However, the CNR contrast did not indicate that either modality was predominantly more sensitive than the other to activity in the temporal poles. Nonetheless, MEG data were localized to anterior temporal lobe regions where fMRI activation was not found. These CNR differences may result from systematically low variance in fMRI data (the noise term of the CNR ratio), even in the presence of weak signals. Finally, the integrated MEG-fMRI activation map and laterality map showed activity in both regions, while neither was apparent when the two were integrated with equal weighting.

As the contrast is a task-specific measure, the weighting scheme is not generalizable beyond the methods employed. With increased computational power, single-trial estimates of activity could be generated at each voxel to assess variance and calculate CNR for individuals. This modification would further optimize the CNR weights across the brain, increasing sensitivity to activity in these regions.

Implementing a weighting system that is influenced by CNR provides several advantages. First, neither activation map is over- or under-represented in the integrated activation map. Rather, the integrated map is the result of a measure of confidence in its constituents. Second, a region that demonstrated activity in both

maps was not provided with additional weight, nor was a region with activity only in one reduced. Provided the maps' respective sensitivity profiles indicated that one modality was primarily sensitive to a region, that modality was represented at near full magnitude in the final result.

4.4 Laterality Mapping for Individuals

In order to integrate MEG and fMRI activation maps for individuals, two requirements must be met. First, conversion of raw signal or a beamformer's pseudo *z* score output to statistical maps necessitates an estimate of within-subject variance. Second, CNR must be calculated for individuals at each voxel. Modeling neural activity for individual trials could meet both of these requirements, but requires high-throughput cluster computing.

Laterality mapping at the individual level provides three notable benefits: the ability to assess surgical candidates using the present method, improved power and sensitivity in all regions, and an estimate of error in CNR maps. While the first two represent an avenue of research with clear clinical utility, the third will be necessary to evaluate the influence of MEG and fMRI on integrated activation maps for various regions.

Integrative laterality mapping at the individual level represents the next step toward multimodal presurgical laterality assessment. It should be noted that this method is not limited to any one type of functional assessment, or any two types of neuroimaging modalities. The integrative framework is universally applicable to any type of volumetric analysis where a noise distribution can be estimated. Furthermore, additional modalities can be recursively implemented, including high-

density EEG activity, positron emission tomography (PET), fMRI or MEG. Application of additional modalities is likely to increase both sensitivity and accuracy.

4.5 Advancing Clinical Effectiveness

Several steps must be made before multimodal neuroimaging can be considered for presurgical assessment. Most notably, this includes an examination of test-retest reliability of the assessment. Additionally, a comparison between active regions and intraoperative stimulation results will substantiate both the findings of individual mapping procedures (MEG and fMRI), and the integration process. It is important to note that the integration framework operates independently of task, and can be applied to a broad range of functional evaluations.

Finally, results should be examined against a comprehensive account of post-surgical outcomes for people with epilepsy, including region of resection, neuropsychological testing results, and seizure type and frequency. This will validate the predictive value of the integrative laterality assessment on a number of axes. While MEG is already being used clinically in a number of centres around the world, validation of these developments will be required in order to employ integrative laterality mapping in a clinical capacity.

4.6 Limitations

As discussed, the present study is limited to production of statistical activation maps using MEG data only at the group level. While a number of studies present MEG activation maps in the form of pseudo *z* scores, this measure is closer in nature to SNR than to *z* scores, and may not be appropriate for conjunction with

fMRI data. Additionally, the necessary loss of MEG timing-related data does not make some group-related differences in activation immediately apparent. Though time series data can be extracted, recovery of time series data is rooted in several parameters, including the time window of interest and significance cutoff, which should be considered carefully.

It is important to note the limitations of functional neuroimaging for application to presurgical evaluation in individuals. Most importantly, there is a known degree of test-retest variability within individuals, and interpretation of these results must be performed with caution. In addition to this, while there is a predictable relationship between neural activity and haemodynamics, fMRI activation may represent venous drainage rather than influx of oxygenated blood to a region, and mislocalization between neural activity, blood flow and magnetic field distribution to some degree is not surprising. Finally, indication of activity via any form of functional neuroimaging does not necessarily demonstrate that a region is critically involved in, or even supporting a function, and resection of fMRI- or MEG-active regions may not prove detrimental to functionality in some cases.

4.7 Future Directions

The next step in integrative laterality mapping will be to develop this procedure for individuals. This will improve on using group-wise weighting factors by accounting for subject-specific differences and allow for estimation of error at the individual level. In addition, both regional activity and CNR distribution across the brain should be validated through repetition, and regional CNR weights can be compared with those derived using different types of tasks. Replication of the

present results represents the most important component of establishing reliability of the measure, and will be required before considering integrative laterality mapping for clinical applications. While regions showing high CNR in both modalities are not likely to change, additional differences may be found in regions not activated by the present task.

As has been discussed, differences remain in the relationship between neural activity, BOLD and electrophysiology. Though these differences are not of evident concern under the present experimental conditions, an optimal method of integration should implement a full model of this relationship at each region in the brain. Such a model has been established as a proof-of-concept using simulated neural activity (Bojak & Oostendorp, 2011). This model renders a population of neurons on the cortical surface, allowing for simultaneous prediction of EEG and fMRI BOLD signals from the underlying mesh. Presently, this model is limited to the limited portions of the cortical surface and requires significant computational power, and has only been applied to simulated data. Future developments will likely strengthen this type of model as an important step toward unification of EEG, MEG and fMRI data.

Finally, the integration framework operates independently of task and modality, with no upper limit on the number that can be integrated at one time. Thus, implementing volumetric activation maps collected using additional neuroimaging modalities may further increase sensitivity and, or open integrative laterality mapping to further applications.

References

Akaike, H. (1974). A new look at the statistical model identification. *IEEE Transactions on Automatic Control*, *19*(6), 716–723. doi:10.1109/TAC.1974.1100705

Al-Otaibi, F., Baeesa, S. S., Parrent, A. G., Girvin, J. P., & Steven, D. (2012). Surgical techniques for the treatment of temporal lobe epilepsy. *Epilepsy research and treatment*, *2012*, 374848. doi:10.1155/2012/374848

Appel, S., Duke, E. S., Martinez, A. R., Khan, O. I., Dustin, I. M., Reeves-Tyer, P., … Theodore, W. H. (2013). Cerebral Blood Flow and fMRI BOLD Auditory Language Activation in Temporal Lobe Epilepsy. *Epilepsia*, *53*(4), 631–638. doi:10.1111/j.1528-1167.2012.03403.x.Cerebral

Bahn, M. M., Lin, W., Silbergeld, D. L., Miller, J. W., Kuppusamy, K., Cook, R. J., … Cross, D. (1997). Localization of language cortices by functional MR imaging compared with intracarotid amobarbital hemispheric sedation. *American journal of roentgenology*, *169*(2), 575–9. doi:10.2214/ajr.169.2.9242780

Bar, M., Tootell, R., Schacter, D., & Greve, D. (2001). Cortical mechanisms specific to explicit visual object recognition. *Neuron*, *29*, 529–535. Retrieved from http://www.sciencedirect.com/science/article/pii/S0896627301002240

Bates, D., Maechler, M., & Bolker, B. (2011). lme4: Linear mixed-effects models using S4 classes. Retrieved from http://cran.r-project.org/package=lme4

Bellgowan, P. S. F., Buffalo, E. A., Bodurka, J., & Martin, A. (2009). Lateralized spatial and object memory encoding in entorhinal and perirhinal cortices. *Learning & Memory*, *16*(7), 433–438. doi:10.1101/lm.1357309.Freely

Binder, J. R., Frost, J. a, Hammeke, T. a, Cox, R. W., Rao, S. M., & Prieto, T. (1997). Human brain language areas identified by functional magnetic resonance imaging. *The Journal of neuroscience*, *17*(1), 353–62. Retrieved from http://www.ncbi.nlm.nih.gov/pubmed/12675261

Binder, J., Swanson, S., Hammeke, T., Morris, G., Mueller, W., Fischer, M., … Haughton, V. (1996). Determination of language dominance using functional MRI: a comparison with the Wada test. *Neurology*, *46*(4), 978–84.

Bogousslavsky, J., Miklossy, J., Deruaz, J. P., Assal, G., & Regli, F. (1987). Lingual and fusiform gyri in visual processing: a clinico-pathologic study of superior altitudinal hemianopia. *Journal of neurology, neurosurgery, and psychiatry*, *50*(5), 607–14. Retrieved from

http://www.pubmedcentral.nih.gov/articlerender.fcgi?artid=1031973&tool=pmcentrez&rendertype=abstract

Bojak, I., & Oostendorp, T. (2011). Towards a model-based integration of co-registered electroencephalography/functional magnetic resonance imaging data with realistic neural population meshes. *Philosophical Transactions of the Royal Society*, *369*, 3785–3801. doi:10.1098/rsta.2011.0080

Bonelli, S. B., Powell, R. H. W., Yogarajah, M., Samson, R. S., Symms, M. R., Thompson, P. J., … Duncan, J. S. (2010). Imaging memory in temporal lobe epilepsy: predicting the effects of temporal lobe resection. *Brain*, *133*(4), 1186–99. doi:10.1093/brain/awq006

Bonelli, S. B., Powell, R., Thompson, P. J., Yogarajah, M., Focke, N. K., Stretton, J., … Koepp, M. J. (2011). Hippocampal activation correlates with visual confrontation naming: fMRI findings in controls and patients with temporal lobe epilepsy. *Epilepsy research*, *95*(3), 246–54. doi:10.1016/j.eplepsyres.2011.04.007

Bookheimer, S. Y., Zeffiro, T. A., Blaxton, T., Gaillard, W., & Theodore, W. (1995). Regional cerebral blood flow during object naming and word reading. *Human Brain Mapping*, *3*(2), 93–106. doi:10.1002/hbm.460030206

Brodie, M. J., Elder, A. T., & Kwan, P. (2009). Epilepsy in later life. *Lancet neurology*, *8*(11), 1019–30. doi:10.1016/S1474-4422(09)70240-6

CANSIM Table 051-0001. (2012). *Statistics Canada*.

Cascino, G. D., Jack, C. R., Parisi, J. E., Sharbrough, F. W., Hirschorn, K. A., Meyer, F. B., … O'Brien, P. C. (1991). Magnetic resonance imaging-based volume studies in temporal lobe epilepsy: pathological correlations. *Annals of neurology*, *30*(1), 31–6. doi:10.1002/ana.410300107

Cavada, C., Compañy, T., Tejedor, J., Cruz-Rizzolo, R. J., & Reinoso-Suárez, F. (2000). The anatomical connections of the macaque monkey orbitofrontal cortex. A review. *Cerebral cortex*, *10*(3), 220–42. Retrieved from http://www.ncbi.nlm.nih.gov/pubmed/10731218

Chen, S., & Li, X. (2012). Functional magnetic resonance imaging for imaging neural activity in the human brain: The annual progress. *Computational and mathematical methods in medicine*. doi:10.1155/2012/613465

Chouinard, P. A., Whitwell, R. L., & Goodale, M. A. (2009). The lateral-occipital and the inferior-frontal cortex play different roles during the naming of visually presented objects. *Human brain mapping*, *30*(12), 3851–64. doi:10.1002/hbm.20812

Cornelissen, P. L., Kringelbach, M. L., Ellis, A. W., Whitney, C., Holliday, I. E., & Hansen, P. C. (2009). Activation of the Left Inferior Frontal Gyrus in the First 200 ms of Reading: Evidence from Magnetoencephalography (MEG). *PLoS ONE*, *4*(4).

Cox, R. W. (1996). AFNI: Software for Analysis and Visualization of Functional Magnetic Resonance Neuroimages. *Computers and Biomedical Research*, *29*(3), 162–173. doi:10.1006/cbmr.1996.0014

D'Arcy, R. C. N., Bardouille, T., Newman, A. J., McWhinney, S. R., Debay, D., Sadler, R. M., … Esser, M. J. (2013). Spatial MEG Laterality maps for language: Clinical applications in epilepsy. *Human Brain Mapping*, *34*(8), 1749–60. doi:10.1002/hbm.22024

Desmond, J. E., Sum, J. M., Wagner, A. D., Demb, J. B., Shear, P. K., Glover, G. H., … Morrell, M. J. (1995). Functional MRI measurement of language lateralization in Wada-tested patients. *Brain: A journal of neurology*, *118 (Pt 6*(Pt 6), 1411–1419. Retrieved from http://www.ncbi.nlm.nih.gov/pubmed/8595473

Devlin, J. T., Russell, R. P., Davis, M. H., Price, C. J., Wilson, J., Moss, H. E., … Tyler, L. K. (2000). Susceptibility-induced loss of signal: comparing PET and fMRI on a semantic task. *NeuroImage*, *11*(6 Pt 1), 589–600. doi:10.1006/nimg.2000.0595

Dixon, P. (2008). Models of accuracy in repeated-measures designs. *Journal of Memory and Language*, *59*(4), 447–456. doi:10.1016/j.jml.2007.11.004

Eldridge, L. L., Engel, S. A., Zeineh, M. M., Bookheimer, S. Y., & Knowlton, B. J. (2005). A dissociation of encoding and retrieval processes in the human hippocampus. *The Journal of neuroscience*, *25*(13), 3280–6. doi:10.1523/JNEUROSCI.3420-04.2005

Epilepsy. (2012). *World Health Organization*. Retrieved August 09, 2013, from http://www.who.int/mediacentre/factsheets/fs999/en/

Finegersh, A., Avedissian, C., Shamim, S., Dustin, I., Paul, M., & Theodore, W. H. (2012). Bilateral hippocampal atrophy in temporal lobe epilepsy: Effect of depressive symptoms and febrile seizures. *Epilepsia*, *52*(4), 689–697. doi:10.1111/j.1528-1167.2010.02928.x.Bilateral

Fisher, R. S., van Emde Boas, W., Blume, W., Elger, C., Genton, P., Lee, P., & Engel, J. (2005). Epileptic seizures and epilepsy: definitions proposed by the International League Against Epilepsy (ILAE) and the International Bureau for Epilepsy (IBE). *Epilepsia*, *46*(4), 470–2. doi:10.1111/j.0013-9580.2005.66104.x

Fox, P. T., & Raichle, M. E. (1986). Focal physiological uncoupling of cerebral blood flow and oxidative metabolism during somatosensory stimulation in human subjects. *Proceedings of the National Academy of Sciences of the United States of*

America, *83*(4), 1140–4. Retrieved from http://www.pubmedcentral.nih.gov/articlerender.fcgi?artid=323027&tool=pmcentrez&rendertype=abstract

Freeman, W. J., Ahlfors, S. P., & Menon, V. (2009). Combining fMRI with EEG and MEG in order to relate patterns of brain activity to cognition. *International Journal of Psychophysiology*, *73*(1), 43–52. Retrieved from http://www.ncbi.nlm.nih.gov/pubmed/19233235

Fuster, J. M. (1997). *The Prefrontal Cortex*. New York: Raven Press.

Geissler, A., Gartus, A., Foki, T., Tahamtan, A. R., Beisteiner, R., & Barth, M. (2007). Contrast-to-noise ratio (CNR) as a quality parameter in fMRI. *Journal of magnetic resonance imaging : JMRI*, *25*(6), 1263–70. doi:10.1002/jmri.20935

Goodale, M. a, & Milner, A. D. (1992). Separate visual pathways for perception and action. *Trends in neurosciences*, *15*(1), 20–5. Retrieved from http://www.ncbi.nlm.nih.gov/pubmed/1374953

Grill-Spector, K., Kourtzi, Z., & Kanwisher, N. (2001). The lateral occipital complex and its role in object recognition. *Vision Research*, *41*, 1409–1422.

Grummich, P., Nimsky, C., & Pauli, E. (2006). Combining fMRI and MEG increases the reliability of presurgical language localization: a clinical study on the difference between and congruence of both modalities. *Neuroimage*, *32*, 1793–1803. doi:10.1016/j.neuroimage.2006.05.034

Hamalainen, M., & Ilmoniemi, R. J. (1994). Interpreting magnetic fields of the brain: minimum norm estimates. *Biomedical Engineering*, *32*, 35–42.

Henry, T. R., Strupp, J. P., & Sikora, M. A. (2011). Hippocampal Sclerosis in Temporal Lobe Epilepsy : Findings at 7 T. *Radiology*, *261*(1), 199–209. doi:10.1148/radiol.11101651/-/DC1

Henson, R. N., Flandin, G., Friston, K. J., & Mattout, J. (2010). A parametric empirical Bayesian framework for fMRI-constrained MEG/EEG source reconstruction. *Human Brain Mapping*, *31*(10), 1512–1531. Retrieved from http://discovery.ucl.ac.uk/167992/

Hertz-Pannier, L., Gaillard, W. D., Mott, S. H., Cuenod, C. A., Bookheimer, S. Y., Weinstein, S., … Theodore, W. H. (1997). Noninvasive assessment of language dominance in children and adolescents with functional MRI: a preliminary study. *Neurology*, *48*(4), 1003–1012. Retrieved from http://www.ncbi.nlm.nih.gov/entrez/query.fcgi?cmd=Retrieve&db=PubMed&dopt=Citation&list_uids=9109891

Huang, M.-X., Lee, R. R., Gaa, K. M., Song, T., Harrington, D. L., Loh, C., … Granholm, E. (2010). Somatosensory System Deficits in Schizophrenia Revealed by MEG during a Median-Nerve Oddball Task. *Brain Topography*, *23*(1), 82–104.

Indefrey, P., & Levelt, W. J. M. (2004). The spatial and temporal signatures of word production components. *Cognition*, *92*(1-2), 101–44. doi:10.1016/j.cognition.2002.06.001

Ingram, J. (2007). *Neurolinguistics : an introduction to spoken language processing and its disorders* (3rd ed., p. 381). Cambridge: Cambridge University Press.

Jenkinson, M., Bannister, P., Brady, M., & Smith, S. (2002). Improved Optimization for the Robust and Accurate Linear Registration and Motion Correction of Brain Images. *NeuroImage*, *17*(2), 825–841. doi:10.1006/nimg.2002.1132

Jeong, W., Chung, C. K., & Kim, J. S. (2012). Localization value of magnetoencephalography interictal spikes in adult nonlesional neocortical epilepsy. *Journal of Korean Medical Science*, *27*(11), 1391–7. doi:10.3346/jkms.2012.27.11.1391

Kobayashi, T., & Kuriki, S. (1999). Principal component elimination method for the improvement of in evoked neuromagnetic field measurements. *IEEE Transactions on Biomedical Engineering*, *46*, 951–958.

Lagerlund, T. D., Shardbrough, F. W., & Busacker, N. E. (1997). Spatial filtering of multichannel electroencephalographic recordings through principal component analysis by singular value decomposition. *Journal of Clinical Neurophysiology*, *14*, 73–82.

Leonard, M. K., Ferjan Ramirez, N., Torres, C., Hatrak, M., Mayberry, R. I., & Halgren, E. (2013). Neural stages of spoken, written, and signed word processing in beginning second language learners. *Frontiers in human neuroscience*, *7*, 322. doi:10.3389/fnhum.2013.00322

Liu, Z., Kecman, F., & He, B. (2006). Effects of fMRI-EEG mismatches in cortical current density estimation integrating fMRI and EEG: a simulation study. *Clinical Neurophysiology*, *117*(7), 1610–1622. Retrieved from http://www.ncbi.nlm.nih.gov/pubmed/16765085

Logothetis, N. K., Pauls, J., Augath, M., Trinath, T., & Oeltermann, A. (2001). Neurophysiological investigation of the basis of the fMRI signal. *Nature*, *412*(6843), 150–7. doi:10.1038/35084005

Maess, B., Herrmann, C. S., Hahne, A., Nakamura, A., & Friederici, A. D. (2006). Localizing the distributed language network responsible for the N400

measured by MEG during auditory sentence processing. *Brain research*, *1096*(1), 163–72. doi:10.1016/j.brainres.2006.04.037

Majos, A., Tybor, K., Stefanczyk, L., & Goraj, B. (2005). Cortical mapping by functional magnetic resonance imaging in patients with brain tumors. *European Radiology*, *15*, 1148–58.

Newman, A. J., Pancheva, R., Ozawa, K., Neville, H. J., & Ullman, M. T. (2001). An event-related fMRI study of syntactic and semantic violations. *Journal of psycholinguistic research*, *30*(3), 339–64. doi:10.1023/A:1010499119393

Nunez, P., & Srinivasan, R. (1981). *Electric fields of the brain: The neurophysics of EEG*. Oxford University Press.

Oishi, M., Kameyama, S., Watanabe, M., Kawaguchi, T., Morota, N., Tomikawa, M., … Tanaka, R. (2002). Presurgical functional mapping of the sensorimotor area using evoked magnetic fields. *No shinkei geka Neurological surgery*. Retrieved from http://www.ncbi.nlm.nih.gov/entrez/query.fcgi?cmd=Retrieve&db=PubMed&dopt=Citation&list_uids=11968825

Oldfield, R. C. (1971). The assessment and analysis of handedness: the Edinburgh inventory. *Neuropsychologia*, *9*(1), 97–113. Retrieved from http://www.ncbi.nlm.nih.gov/pubmed/5146491

Pang, E. W., Wang, F., Malone, M., Kadis, D. S., & Donner, E. J. (2011). Localization of Broca's area using verb generation tasks in the MEG: validation against fMRI. *Neuroscience letters*, *490*(3), 215–9. doi:10.1016/j.neulet.2010.12.055

R Development Core Team. (2008). *R: A Language and Environment for Statistical Computing*. Vienna, Austria: R Foundation for Statistical Computing.

Rees, G., Howseman, A., Josephs, O., Frith, C. D., Friston, K. J., Frackowiak, R. S., & Turner, R. (1997). Characterizing the relationship between BOLD contrast and regional cerebral blood flow measurements by varying the stimulus presentation rate. *NeuroImage*, *6*(4), 270–8. doi:10.1006/nimg.1997.0300

Rostrup, E., Law, I., Blinkenberg, M., Larsson, H. B., Born, A. P., Holm, S., & Paulson, O. B. (2000). Regional differences in the CBF and BOLD responses to hypercapnia: a combined PET and fMRI study. *NeuroImage*, *11*(2), 87–97. doi:10.1006/nimg.1999.0526

Roux, F. E., Boulanouar, K., Ibarrola, D., Tremoulet, M., Chollet, F., & Berry, I. (2000). Functional MRI and intraoperative brain mapping to evaluate brain plasticity in patients with brain tumours and hemiparesis. *Journal of Neurology, Neurosurgery & Psychiatry*, *69*(4), 453–463. Retrieved from

http://www.pubmedcentral.nih.gov/articlerender.fcgi?artid=1737155&tool=pmcentrez&rendertype=abstract

Schacter, D., Gilbert, D., & Wegner, D. (2011). *Psychology* (2nd ed., pp. 364–366). New York: Worth Publishers.

Sekihara, K., Nagarajan, S. S., Poeppel, D., & Marantz, A. (2004). Asymptotic SNR of Scalar and Vector Minimum-Variance Beamformers for Neuromagnetic Source Reconstruction. *IEEE Transactions on Biomedical Engineering*, *51*(10), 1726–1734.

Sidhu, M. K., Stretton, J., Winston, G. P., Bonelli, S., Centeno, M., Vollmar, C., … Duncan, J. S. (2013). A functional magnetic resonance imaging study mapping the episodic memory encoding network in temporal lobe epilepsy. *Brain*, *136*, 1868–1888. doi:10.1093/brain/awt099

Smith, S. M. (2002). Fast Robust Automated Brain Extraction. *Human Brain Mapping*, *17*, 143–155. doi:10.1002/hbm.10062

Smith, S. M., Jenkinson, M., Woolrich, M. W., Beckmann, C. F., Behrens, T. E. J., Johansen-Berg, H., … Matthews, P. M. (2004). Advances in functional and structural MR image analysis and implementation as FSL. *NeuroImage*, *23 Suppl 1*, S208–19. doi:10.1016/j.neuroimage.2004.07.051

Squire, L. R. (1992). Memory and the hippocampus: a synthesis from findings with rats, monkeys, and humans. *Psychological review*, *99*(2), 195–231. Retrieved from http://www.ncbi.nlm.nih.gov/pubmed/1594723

Stretton, J., Winston, G., Sidhu, M., Centeno, M., Vollmar, C., Bonelli, S., … Thompson, P. J. (2012). Neural correlates of working memory in Temporal Lobe Epilepsy--an fMRI study. *NeuroImage*, *60*(3), 1696–703. doi:10.1016/j.neuroimage.2012.01.126

Talairach, J., & Tournoux, P. (1988). *Co-planar Stereotaxic Atlas of the Human Brain: 3-Dimensional Proportional System - an Approach to Cerebral Imaging*. New York: Thieme Medical Publishers.

Taulu, S., Kajola, M., & Simola, J. (2004). Suppression of interference and artifacts by the signal space separation method. *Brain Topography*, *16*(269), 275.

Tremblay, A., & Ransijn, J. (2013). LMERConvenienceFunctions: A suite of functions to back-fit fixed effects and forward-fit random effects, as well as other miscellaneous functions.

Vrba, J., Taulu, S., & Nenonen, J. (2010). Signal Space Separation Beamformer. *Brain Topography*, *23*, 128–133. doi:10.1007/s10548-009-0120-7

Wada, J. (1949). A new method for the determination of the side of cerebral speech dominance. A preliminary report of the intra-carotid injection of sodium amytal in man. *Igaku to Seibutsugaki*, *14*, 221–222.

Wiebe, S. (2000). Epidemiology of temporal lobe epilepsy. *The Canadian Journal of Neurological Sciences*, *27*, S20–1.

Wiebe, S., Blume, W. T., Girvin, J. P., & Eliasziw, M. (2001). A randomized, controlled trial of surgery for temporal-lobe epilepsy. *The New England journal of medicine*, *345*(5), 311–8. doi:10.1056/NEJM200108023450501

Williams, E. J., Stretton, J., Centeno, M., Bartlett, P., Burdett, J., Symms, M., … Micallef, C. (2012). Clinical language fMRI with real-time monitoring in temporal lobe epilepsy: Online processing methods. *Epilepsy & Behavior*, *25*(1), 120–124.

Woermann, F. G., Jokeit, H., Luerding, R., Freitag, H., Schulz, R., Guertler, S., … Ebner, A. (2003). Language lateralization by Wada test and fMRI in 100 patients with epilepsy. *Neurology*, *61*(5), 699–701. Retrieved from http://www.ncbi.nlm.nih.gov/pubmed/12963768

Woolrich, M. W., Ripley, B. D., Brady, M., & Smith, S. M. (2001). Temporal Autocorrelation in Univariate Linear Modeling of FMRI Data. *NeuroImage*, *14*, 1370–1386. doi:10.1006/nimg.2001.0931

Zeffiro, T. (1996). Clinical functional image analysis: artifact detection and reduction. *NeuroImage*, *4*(3 Pt 3), S95–100. doi:10.1006/nimg.1996.0059

Appendix A: Post-Surgical Outcomes

Case One

The first participant to receive surgery was right-handed with a right-hemisphere seizure focus. Prior to surgery, this person demonstrated atypical right-lateralized speech dominance as indicated by a dichotic listening task, and tested normally for verbal IQ and verbal memory. However, they also showed impairments in visuospatial and constructional skills. This pattern is consistent with damage to the right hemisphere. The individual's integrated MEG-fMRI activation map can be seen in Figure 13.

The participant underwent a right anterior temporal lobe resection. They demonstrated no change in language abilities, and an increase in verbal memory. The time between the first and second assessments was two years, with surgery following the first assessment by ten months. A reduction in language abilities was initially expected due to right-hemisphere lateralization, but this did not occur. While the task used did not exclusively elicit language activation, its demands include verbal processing. Thus, Figure 13 coincides with outcomes, as right-hemisphere dominance is shown but with no significantly active clusters in the resected region.

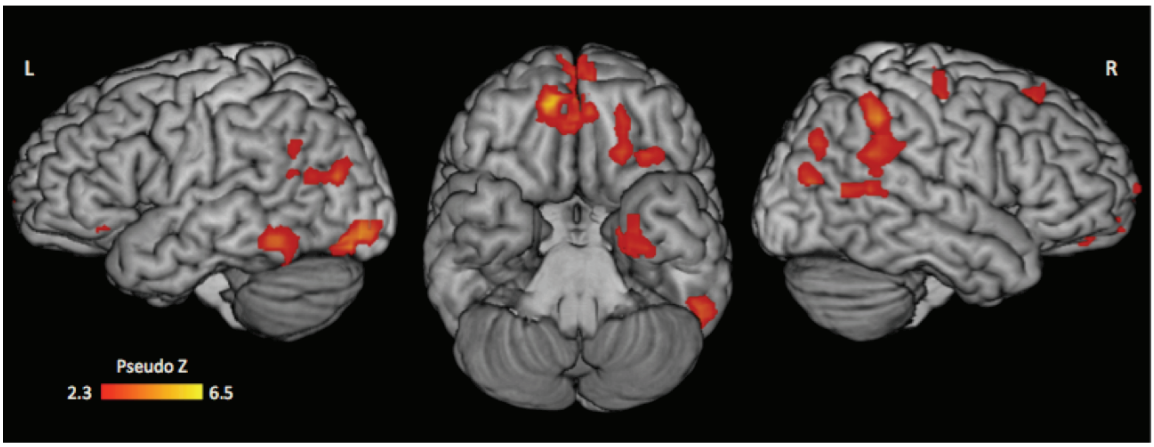

Figure 14 Integrated MEG-fMRI activation map for the first participant to undergo surgery. Activation is thresholded at a pseudo *z* value of 2.3, with a minimum cluster size of 250 voxels.

Case Two

The second participant was right-handed and showed a right-ear advantage in a dichotic listening task, indicating left-hemisphere language lateralization. They showed a left temporal seizure focus and average verbal memory functioning. The time between the first and second assessments was two years, with surgery following the first assessment by eight months.

The participant underwent a left temporal lobectomy, and subsequently showed impairments in verbal memory functioning, as well as a slight decline in confrontation name and oral fluency. These results are common for a temporal lobectomy in the dominant hemisphere. The participant's activation shown in Figure 14 depicts a bilaterally distributed set of active regions, with numerous clusters in the left hemisphere, including the middle temporal gyrus. This pattern of activation

is consistent with the outcome, as activation aligns with the region of resection and is predictive of a performance decrease in confrontation naming.

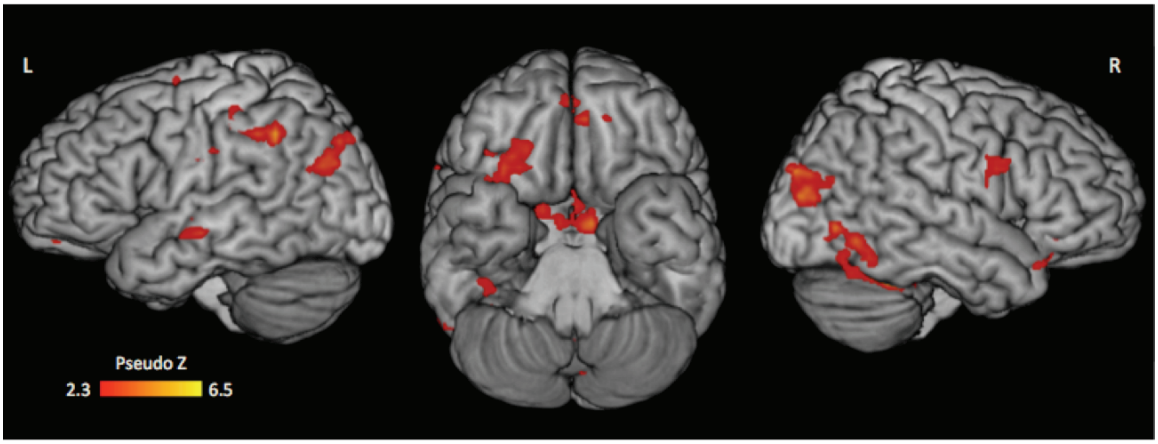

Figure 15 Integrated MEG-fMRI activation map for the second participant to undergo surgery. Activation is thresholded at a pseudo *z* value of 2.3, with a minimum cluster size of 250 voxels.